Available online at www.sciencedirect.com
ScienceDirect
Lithos 99 (2007) 151–177
LITHOS
www.elsevier.com/locate/lithos

Magmatic relationships and ages between adakites, magnesian andesites and Nb-enriched basalt-andesites from Hispaniola: Record of a major change in the Caribbean island arc magma sources

J. Escuder Viruete [a,*], F. Contreras [b], G. Stein [c], P. Urien [c], M. Joubert [c], A. Pérez-Estaún [d], R. Friedman [e], T. Ullrich [e]

[a] *Instituto Geológico y Minero de España, C. Ríos Rosas 23, 28003 Madrid. Spain*
[b] *INYPSA. C. G. Díaz porlier - 49. 28001 Madrid. Spain*
[c] *BRGM. Av. C. Guillemin. 45060 Orléans. France*
[d] *I.C.T. Jaume Almera-CSIC. C. Lluís Solé i Sabarís s/n. 08028 Barcelona. Spain*
[e] *Pacific Centre for Isotopic and Geochemical Research. University of British Columbia, 6339 Stores Road Vancouver, Canada BC V6T 1Z4*

Received 29 September 2006; accepted 26 January 2007
Available online 1 February 2007

Abstract

Located in the Cordillera Central of the Dominican Republic, the Late Cretaceous Tireo Fm (TF) records a major change of the magma sources in the Caribbean island arc. It comprises a >3 km thick sequence of arc-related volcanic and volcano-sedimentary rocks with variable geochemical characteristics. Combined detailed mapping, stratigraphy, geochemistry and U–Pb/Ar–Ar geochronology show that the volcanic rocks of the Tireo Fm include two main volcanic sequences. The lower volcanic sequence is dominated by monotonous submarine vitric–lithic tuffs and volcanic breccias of andesite to basaltic andesite, with minor interbedded flows of basalts and andesites. Fossil and (U–Pb and ^{40}Ar–^{39}Ar) geochronological data show that arc magmatism in the lower sequence began to accumulate before ~ 90 Ma, from the Aptian to Turonian. These rocks constitute an island arc tholeiitic suite, derived from melting by fluxing of a mantle wedge with subduction-related hydrous fluids. The upper volcanic sequence is characterized by a spatial and temporal association of adakites, high-Mg andesites, and Nb-enriched basalts, which collectivelly define a shift in the composition of the subduction-related erupted lavas. A dacitic to rhyolitic explosive volcanism with subaerial and episodic aerial eruptions, and sub-volcanic emplacements of domes, characterize mainly this stratigraphic interval. The onset of this volcanism took place at Turonian–Coniacian boundary and continued in the Santonian to Lower Campanian, with minor events in the Late Campanian. Adakites represent melts of the subducting slab, magnesian andesites the product of hybridization of adakite liquids with mantle peridotite, and Nb-enriched basalts melts of the residue from hybridization. We propose a model of oblique ridge subduction at ~ 90 Ma and possibly subsequent slab window formation, as principal cause of magmatic variations recorded in the Caribbean island arc, above a southwestern-dipping subduction zone.
© 2007 Elsevier B.V. All rights reserved.

Keywords: Subduction; Adakites; Nb-enriched basalts; Magnesium andesites; Caribbean island arc

* Corresponding author. Instituto Geológico y Minero de España. Geología y Geofísica. C. La Calera 1, 28760 Tres Cantos, Madrid. Spain. Tel.: +34 917287242.
E-mail addresses: j.escuder@igme.es, escuder@geo.ucm.es (J. Escuder Viruete).

0024-4937/$ - see front matter © 2007 Elsevier B.V. All rights reserved.
doi:10.1016/j.lithos.2007.01.008

1. Introduction

Intra-oceanic subduction zones are the Earth's geologic environments where continuous consumption of oceanic lithosphere occurs toward final arc-continent collision. In these settings, the fluid phase released by the dehydration of the downgoing slab is a viable agent for slab-to-mantle element transfer, mantle metasomatism and melting. The composition of the metasomatized mantle and the dynamics of the mantle wedge ultimately control magma production at subduction zones and the distinctive trace element features of arc magmas (Pearce and Parkinson, 1993; Tatsumi and Eggins, 1995; Stern, 2002). Under normal arc conditions, subduction zone magmas are generated by partial melting in the metasomatized mantle source (e.g., Tatsumi, 1989; Pearce and Peate, 1995). However, when young (<5 Ma), and hot, oceanic lithosphere is subducted, it may melt under garnet amphibolite to eclogite facies conditions and produce high-Al trondhjemite melts, termed adakites (Defant and Drummond, 1990, 1993; Drummond and Defant, 1990; Kepezhinskas et al., 1996; Yogodzinski et al., 2001).

The occurrence of adakites, magnesian andesites and Nb-enriched basalts, in association with "normal" tholeiitic to calc-alkaline subduction-related suites, has been described in several arcs, as Mindanao and Zamboanga (Philippines), Central and South America (Mexico, Panamá and Ecuador), Aleutians and North Kamchatka (Defant et al., 1991; Maury et al., 1996; Sajona et al., 1996; Yogodzinski et al., 2001; Bourdon et al., 2002; Calmus et al., 2003). This association has been interpreted as the result of a subduction zone magma production, where adakites represent melts of the subducting slab, magnesian andesites the product of hybridization of adakite liquids with mantle peridotite, and Nb-enriched basalts melts of the hybridized residue (Kelemen et al., 1990; Defant and Drummond, 1990; Kepezhinskas et al., 1996; Drummond et al., 1996; Martin et al., 2005).

The Late Cretaceous Tireo Fm (Cordillera Central of Hispaniola) contains magnesian andesites, Nb-enriched basalts and andesites, and adakites (dacites to rhyolites), in association with tholeiitic to calc-alkaline basalt-andesite arc-related volcanic and volcaniclastic sequences. Compositional boundaries between these suites are transitional. Because this magmatic association is well constrained in a plate-tectonic context, the Tireo Fm is therefore a key element for understanding the magma sources and subduction zone petrogenetic processes in the Caribbean island arc during the Late Cretaceous. As part of the Cartographic Program of the Dominican Republic funded by the European Union (SYSMIN project) an integrated study of detailed mapping, stratigraphy, geochemistry and U–Pb/Ar–Ar geochronology of the Tireo Fm has been carried out. A geochemical traverse of the Late Cretaceous Caribbean island arc has been acquired in the areas (Fig. 1): Restauración-Jicomé, including the Dajabón Complex of Draper and Lewis (1991); Monción-Lamedero; Jarabacoa; and Gajo del Monte-Constanza. This study shows that the volcanic rocks of the Tireo Fm record a major change in composition from tholeiitic to low-K calc-alkaline "normal" basalts and andesites in the lower volcanic sequence, toward an association of adakites, magnesium andesites and Nb-enriched basalts in the upper volcanic sequence. The geological, geochemical and geochronological data of this magmatic association, provide support for a tectonomagmatic model of spreading ridge subduction beneath the Hispaniola segment of the Caribbean island arc at the Turonian–Coniacian boundary (~ 89 Ma).

2. Geological setting

Located on the northern margin of the Caribbean plate, the tectonic collage of Hispaniola results from the WSW to SW-directed oblique-convergence of the continental margin of the North American plate with the Cretaceous Caribbean island arc system, which began in Eocene to Early Miocene times and continues today (see review by Mann, 1999). The arc-related rocks are regionally overlain by Upper Eocene to Holocene siliciclastic and carbonate sedimentary rocks that post-date island arc activity, and record the oblique arc–continent collision in the north, as well as the active subduction in the southern Hispaniola margin. Central Hispaniola is a composite of oceanic derived units bound by the left-lateral strike-slip Hispaniola (HFZ) and Bonao-La Guácara (BGFZ) fault zones (Fig. 1). Accreted units mainly include: the Loma Caribe peridotite, MORB-type gabbros and basalts, and Late Jurassic pelagic sediments; the Lower Cretaceous oceanic plateau of the Duarte Complex; and the Late Cretaceous arc-related igneous and metamorphic rocks of the Tireo Fm (Bowin, 1975; Lewis et al., 1991; Lapierre et al., 1999; Lewis et al., 2002; Escuder Viruete et al., 2004, in press). Central Hispaniola underwent deformation by regional sinistral transpressive and transtensive regime during the Coniacian–Santonian (90–84 Ma) to the Middle Campanian (77–74 Ma), and was accompanied by the intrusion of syn- to late-kinematic gabbro-tonalitic batholiths (Escuder Viruete et al., 2006a). Sedimentary basins filled with the Magua-Tavera Fm

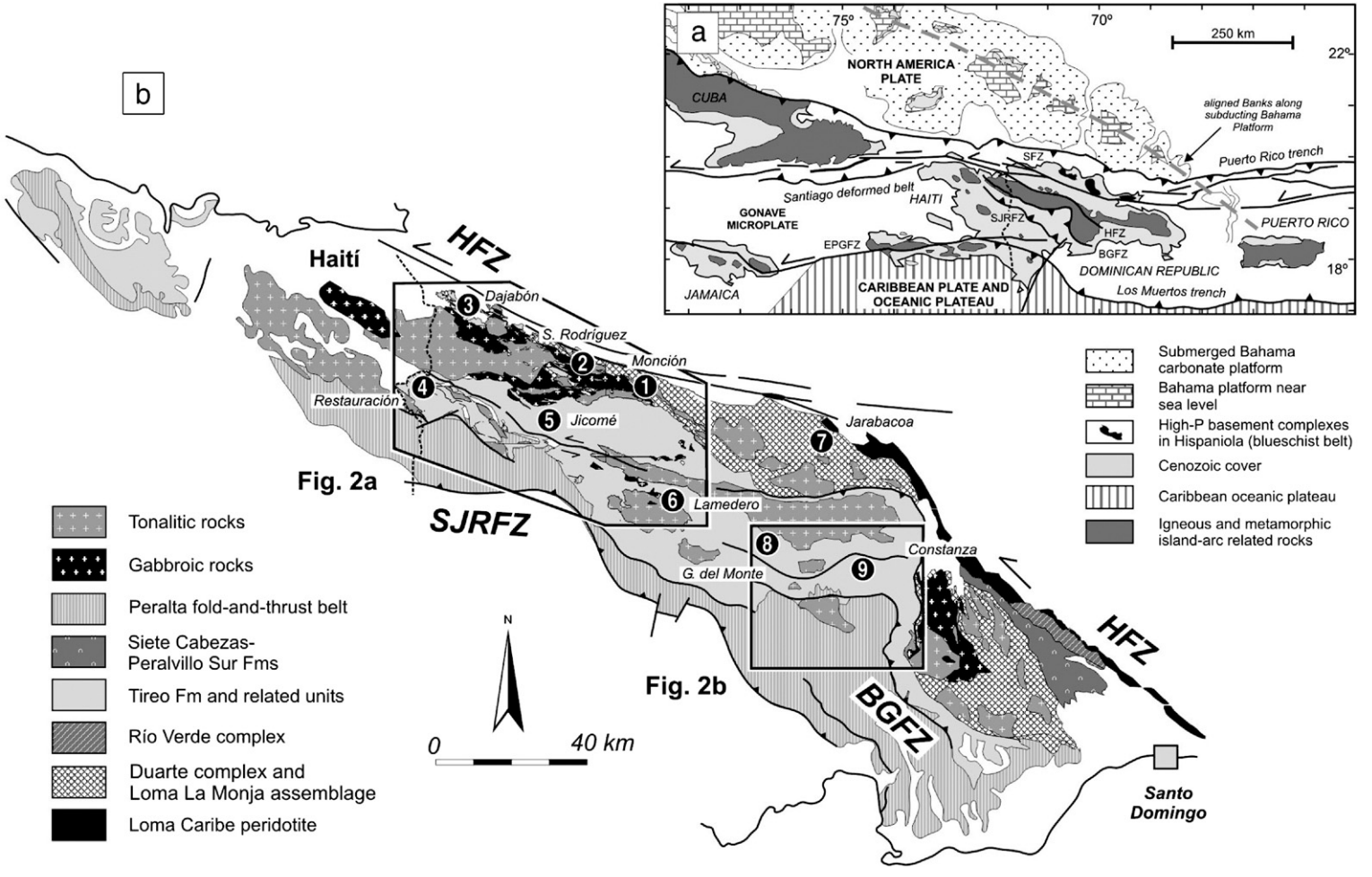


Fig. 1. (a) Map of the northeastern Caribbean plate margin modified from Mann (1999); (b) Schematic geological map of Central Hispaniola. SFZ=Septentrional fault zone; HFZ=Hispaniola fault zone; BGFZ=Bonao-La Guácara fault zone; SJRFZ=San Juan–Restauración fault zone; EPGFZ=Enriquillo–Plantain Garden fault zone. Box shows map of the Tireo Fm in Fig. 2a and b. Encircled number show location of lithostratigraphic columns of the Tireo Fm in Fig. 3.

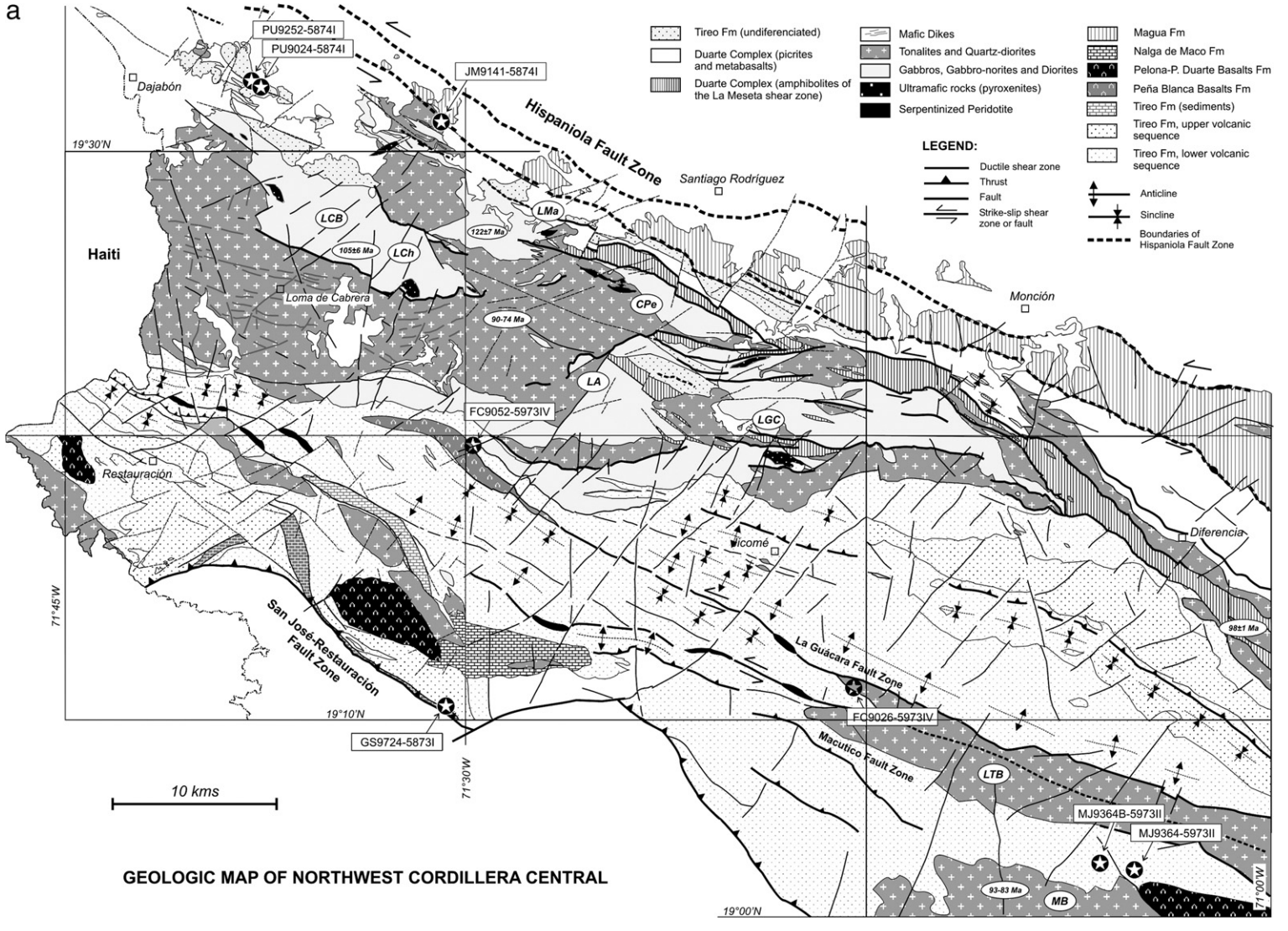


Fig. 2. (a) Geological map of the NW Cordillera Central, Dominican Republic (Contreras et al., 2004; Stein et al., 2004). LCB=Loma de Cabrera batholith; LTB=Loma del Tambor batholith; MB=Macutico batholith. Ultramafic-gabbroic massifs: Loma Chacuey (LCh), Loma los Mameyes (LMa), Cerro del Pescado (CPe), Lomas Altas (LA) and Loma Guazumito-Los Charamicos (LGC). Text labels in boxes show location of samples selected for U–Pb and $^{40}Ar/^{39}Ar$-geochronology. (b) Geological map of the Constanza area in the Cordillera Central (mod. from Gómez Sáinz, 2000).

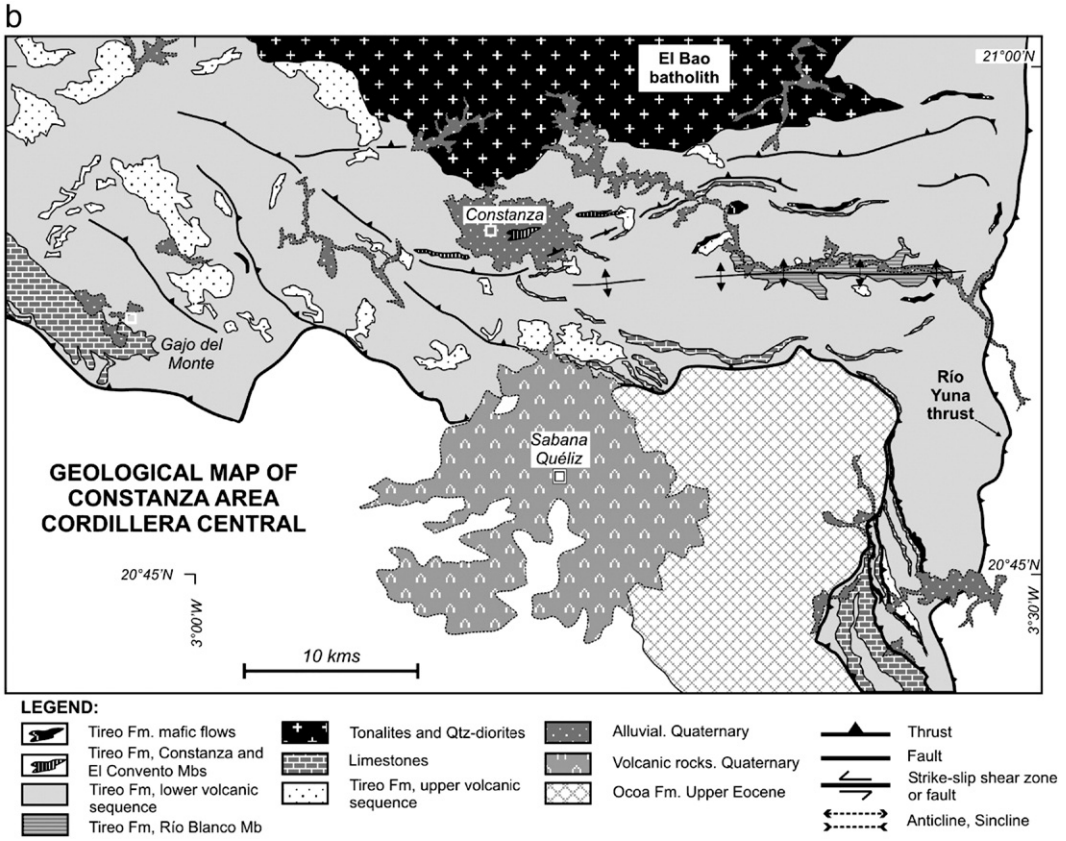


Fig. 2 (*continued*).

(Contreras et al., 2004) and unconformably deposited over these units, indicates that the main ductile structure of Central Hispaniola was pre-Eocene/Oligocene.

In the study area of Cordillera Central, six lithostratigraphic and geochemical units have been mapped (Contreras et al., 2004; Stein et al., 2004). They include, from bottom to top (Fig. 2): (1) the Loma Caribe serpentinized peridotite; (2) the Loma La Monja volcano-plutonic assemblage; (3) the El Aguacate Chert; (4) the Duarte Complex; (5) the Tireo Fm; (6) and Peña Blanca Fm basalts. All these units underwent variable deformation and metamorphism. The Loma Caribe peridotite consists of serpentinized harzburgite, dunite and lherzolite, with dykes and tectonic blocks of gabbro and dolerite. The Loma La Monja volcano-plutonic assemblage consists of a <3-km thick sequence of isotropic gabbros, minor cumulate-layered olivine gabbros, massive Fe–Ti basalts and dolerites that grade upward into pillow lavas, and are overlain by phyric basalts, sediments and the El Aguacate Chert. The El Aguacate Chert consists of 150-m thick sequence of ribbon chert with radiolarian microfauna of Oxfordian to Tithonian age (Montgomery and Pessagno, 1999). The Duarte Complex includes picrites, high-Mg basalts and basalts that recorded an (>96 Ma) Early Cretaceous phase of construction of the Caribbean–Colombian oceanic plateau (CCOP; Lapierre et al., 1999; Kerr et al., 2002; Escuder Viruete et al., in press). The Peña Blanca Fm comprises mostly massive aphyric basalts that overlie the Tireo Fm. Their Campanian s.l. age and geochemical characteristics (enriched tholeiitic basalts with flat REE patterns) permitted to attribute this unit to the CCOP (Escuder Viruete et al., 2004).

3. Previous work

The Late Cretaceous Tireo Fm form part of the "mature" Caribbean island arc (Donnelly et al., 1990; Lewis et al., 1991; Lebrón and Perfit, 1994; Jolly et al., 1998, 2001; Lewis et al., 2002, Jolly and Lidiak, 2006). Donnelly et al. (1990) used the term "mature" to describe the plutonic, volcanic and volcanoclastic rocks of the Tireo Fm and similar calc-alkaline Caribbean volcanic rock suites that, respect to the previous tholeiitic primitive magmas, have: (1) a greater enrichment in LILE and LREE; (2) an upper $^{87}Sr/^{86}Sr$ and lower $^{143}Nd/^{144}Nd$ isotopic ratios; (3) and a characteristic $^{206}Pb/^{204}Pb$

composition derived from a subducted sedimentary component. Microfossil data reported by Bowin (1975) indicated a Cenomanian to Maastrichtian age for the formation. Lewis et al. (1991) grouped the Late Cretaceous volcanic and volcaniclastic rocks in a Tireo Group, which forms a continuous 300-km long belt that extends along the Cordillera Central in the Dominican Republic and the Massif du Nord in Haiti (Fig. 1). These authors divided the Tireo Group into two main units, where the sedimentary intercalations were informally separated into members (Mb). The lower unit include a thick sequence of vitric–lithic tuffs with intercalated mafic flows and sediments. Microfossil content in limestones and cherts indicate a late Cenomanian–Turonian to early Senonian age for the volcanism (Fig. 3; Gómez Sáinz, 2000). The upper unit consists of dacitic to rhyolitic lavas and pyroclastic rocks of Late Santonian to Early Campanian age (Lewis et al., 1991). The Tireo Group is unconformably overlain by turbiditic marine sediments of Middle to Late Campanian to Maastrichtian age of the Trois Rivières Fm.

4. Geology of the Tireo Fm

New mapping allows to establish that the Tireo Fm comprises a >3 km thick sequence of arc-related volcanic, subvolcanic and volcano-sedimentary rocks, with variable geochemical characteristics, which is intruded by gabbro-diorite to Hbl-bearing tonalite batholiths, including ultramafic complexes. Following Lewis et al. (1991), two main volcanic sequences have been mapped in the Cordillera Central (Figs. 2, 3).

4.1. Lower volcanic sequence

The lower volcanic sequence is dominated by coarse tuffs, lapilli tuffs and volcanic breccias of mainly andesite, with locally interbedded basaltic flows. With a thickness of >2500 m, this extensive pyroclastic sequence crop out continually from the Restauración-Jicomé to the Gajo del Monte-Constanza areas. Towards the NE (Monción-Jarabacoa areas), however, the lower volcanic sequence is not present. The tuffs are massive or poorly stratified in thick beds, poorly sorted, and composed of green to gray lithic fragments, and yellow-brown angular, devitrified glass shards, and <2% of crystal fragments of pyroxene, plagioclase and hornblende. Quartz-bearing clasts are absent. These rocks erupted and partially reworked as debris flows in a relatively deep-water submarine environment. However, interbedded decimeter-thick layers of accretionary lapilli locally occur (SW Restauración), which were deposited in relatively shallow water transitional to a subaerial environment. Andesites are characterized by glomeroporphyritic pyroxene, plagioclase and iron oxide. Massive, porphyritic to aphyric, dark-green basaltic lavas are present toward the base of the sequence. Local microgabbros and dolerites are interpreted as the internal part of lobes and syn-volcanic feeder dykes. Discontinuous intercalations of sedimentary rocks occur at the base and top of the lower volcanic sequence (Fig. 3). Radiolarian fossils in cherts of the lowermost stratigraphical levels of the Dajabón complex, suggest Albian to Upper Cenomanian times for the onset of arc volcanism (Montgomery and Pessagno, 1999). This age is consistent with the Albian–Cenomanian age for the turbiditic Río Blanco Mb (Gómez Sáinz, 2000). Foraminifera content in the Constanza Mb and limestones at Restauración indicate a pre-Turonian age for the underlying lower volcanic sequence (Bowin, 1975; Lewis et al., 1991). Taken together, these ages indicate an Albian–Cenomanian (112–99 Ma) age for the lower volcanic sequence.

4.2. Upper volcanic sequence

The upper volcanic sequence (Fig. 3) is composed by dacite to rhyolite flows, tuffs and tuff breccias, extrusive dacite domes, and domal to dyke-like intrusive bodies of fine-grained rhyolites. The sequence have interbedded mafic flows and sediments, and is intruded by basaltic to dolerite dykes. The acid rocks erupted as shallow submarine flows and pyroclastic deposits produced by phreatomagmatic explosions, with local subvolcanic intrusions. A late stage hydrothermal activity has taken place within the acidic rock centers, producing significant epithermal polymetallic Cu–Au–Ag sulfide-barite deposits. Dacites are porphyritic with abundant plagioclase and hornblende, rare clinopyroxene and embayed quartz phenocrysts. Rhyolites are characterized by quartz, K-feldspar and plagioclase phenocrysts. The upper unit has a thickness of about 600–1500 m in the Dajabón, Restauración and Jicomé areas and pinches out toward the SE in the Gajo del Monte, Constanza and Sabana Quéliz areas. The age of the upper volcanic sequence is not well constrained. Fragments of green andesite within the dacite tuffs indicates a younger age for the upper volcanic sequence. At Restauración, discontinuous limestone intercalations on top of the crystal-lithic tuff sequence yields from microfossils a Turonian age and a plateau Ar–Ar age for hornblende of 81.2±8.2 has been obtained for dacite (Lewis et al., 1991).

5. Geochronology

The U–Pb and $^{40}Ar/^{39}Ar$ ages for selected rocks of the Tireo Fm and related intrusives are presented below. The

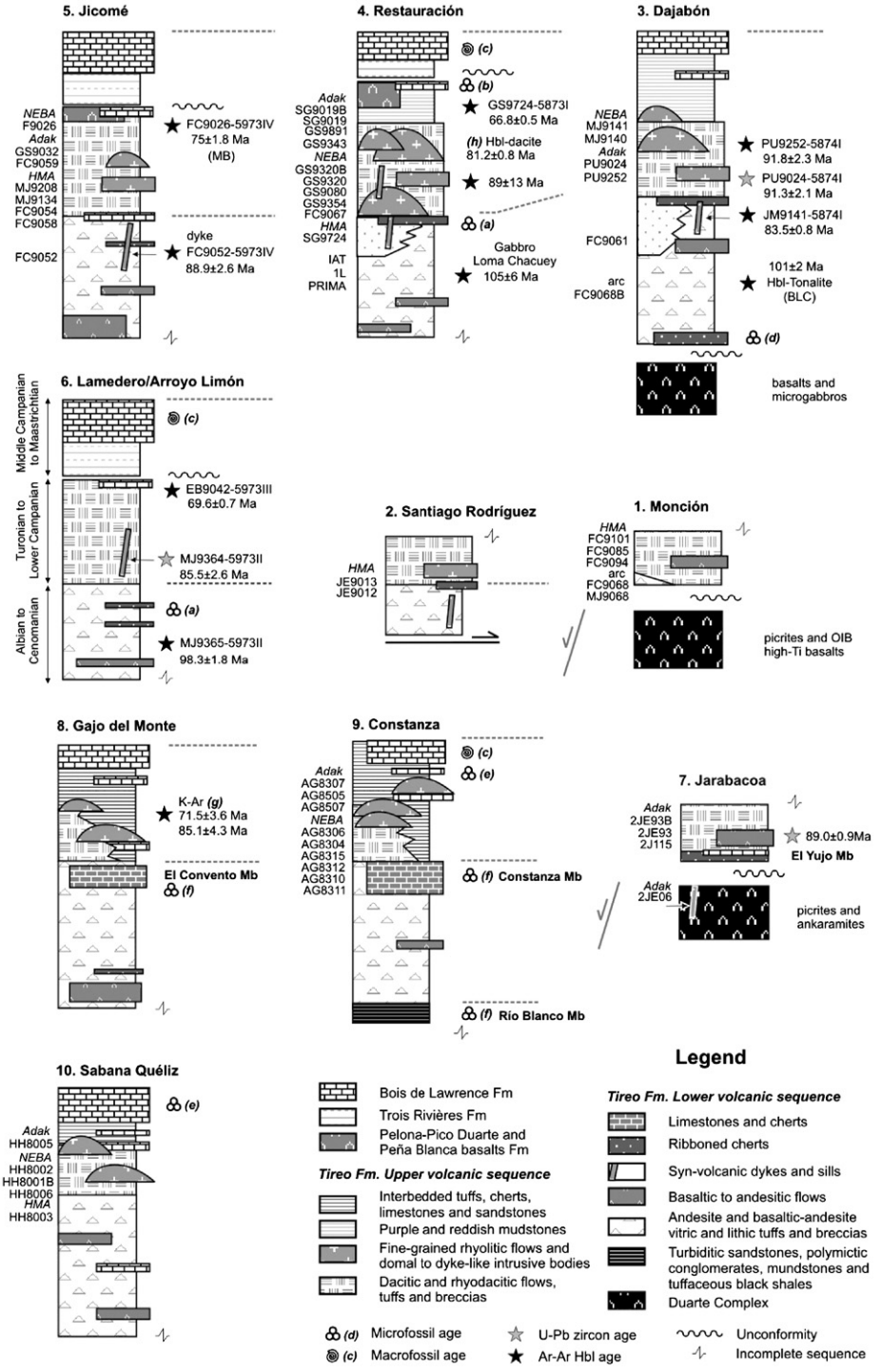


Fig. 3. Schematic lithostratigraphic columns of the Tireo Fm. Location is show in Fig. 1. Stars show locations of samples for U–Pb and $^{40}Ar/^{39}Ar$ geochronology. Age data: (a) Montgomery and Pessagno (1999); (b) Stein et al. (2004); (c) Bowin (1975); (d) Escuder Viruete et al. (2004); (e) Lewis et al. (1991); (f) Gómez Sáinz (2000). Location of selected samples of each geochemical group is also show. Adak = adakites; HMA = high-Mg andesites; NEBA = Nb-enriched basalts and andesites.

geological map of Fig. 2a indicates the sample locations. Analytical procedures are in the online version of this article; see Appendix A. All ages are quoted at the 2σ level of uncertainty.

5.1. U–Pb samples

A porphyritic rhyolite flow, with K-feldspar+albite+quartz phenocrysts and minor biotite, of the upper volcanic sequence in the Dajabón area (PU9024-5874I), and a hornblende+plagioclase-phyric andesite dyke in the Lamedero area (MJ9364-5973II) were dated. The rhyolite flow has adakitic affinity and is located in the lowermost stratigraphic levels of the upper sequence. Separated zircon grains are clear, colorless euhedral prismatic prisms, with aspect ratios of ~ 1.5–3.5. The age was determined from four abraded zircon fractions (A to D), which are all concordant (Fig. 4a) and give an age of 91.3±2.1 Ma (Appendix 2). This Turonian (geologic time scale from Gradstein et al., 2004) age is interpreted as the crystallization age of the sample. The andesite dyke is Nb-rich and intrusive in the lower volcanic sequence. Zircon grains are clear, pale pink, stubby to elongate prisms, with aspect ratios of ~ 1.5–2.0. Zircon fractions D and C are discordant, showing evidence for inherited zircon. Fractions A and B are concordant (Fig. 4b) and give an age of 85.5±2.6 Ma. This Coniacian–Santonian boundary age is interpreted as the crystallization age.

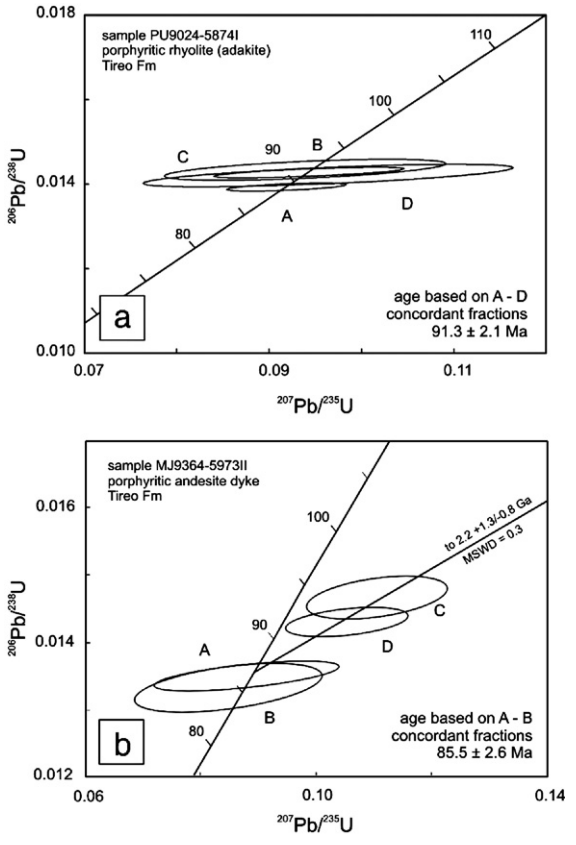


Fig. 4. Concordia diagrams for (a) porphyritic rhyolite (adakite) of the upper volcanic sequence in the Dajabón sheet area (PU9024-5874I) and (b) porphyritic andesite dyke located in the Lamedero sheet area (MJ9364-5973II). U–Pb procedures and analytical data are in the Appendices 1 and 2. See text for discussion.

5.2. $^{40}Ar/^{39}Ar$ samples

Hornblende-bearing porphyritic andesites, dacites and rhyolites of the upper volcanic sequence, and related tonalite dykes were selected for $^{40}Ar/^{39}Ar$ dating (Figs. 3 and 5; Appendix 3). The $^{40}Ar/^{39}Ar$ ages are interpreted as cooling ages after extrusion of the magmas or emplacement of the intrusions. Sample PU9252-5874I is an unfoliated rhyodacitic flow (adakite), spatially equivalent with the rhyolite sample dated by U–Pb methods. For four steps (5–8), the obtained plateau age from hornblende is 91.8±2.3 Ma representing 73.5% of the ^{39}Ar released. The inverse isochron age on eight points is 92.2±10 Ma. Sample MJ9364B-5973II is a hornblende+plagioclase high-Mg andesitic dyke with porphyritic texture, intrusive in the lower volcanic sequence in the Lamedero area. For seven steps (2–8), the obtained hornblende plateau age from hornblende is 88.6±1.8 Ma for 98.7% of the ^{39}Ar released. The inverse isochron age is 89.5± 5.6 Ma. Sample MJ9141-5874I is a hornblende tonalite dyke (Nb=11 ppm) that intrudes and cross-cuts the Duarte Complex in the Dajabón area. Very probably, this dike is an apophisis of the Loma de Cabrera batholith. For six steps (4–9), the obtained plateau age from hornblende is 83.5±0.8 Ma for 94.2% of the ^{39}Ar released. Inverse isochron age is 85.2±2.5 Ma. Sample FC9052-5973IV is an unfoliated hornblende+plagioclase-phyric andesite dike (Nb=7.2 ppm), intrusive in the Duarte Complex in the Jicomé area. For six steps (4–10), the obtained hornblende plateau age from hornblende is 88.9±2.6 Ma for 92.9% of the ^{39}Ar released. The inverse isochron age is 90.2±7.5 Ma. Sample EB9042-5973III is a biotite-bearing porphyritic late andesite in the Arroyo Limón area. The sample yielded a plateau age for biotite of 69.6± 0.7 Ma for the high temperature six steps (6–11) and 72.3% of the ^{39}Ar released. Inverse isochron age is 70.9± 2.2 Ma. Sample GS9724-5873I is a high-Mg hornblende-phyric andesitic flow of the upper sequence in the Restauración area. This sample yielded an imprecise plateau age for hornblende of 98±17 Ma (all steps). In the same sample, the obtained plateau age from K-feldspar is 66.8± 0.47 Ma for six steps (3–7) and 83.3% of the ^{39}Ar released. The inverse isochron age is 67.5±2.1 Ma.

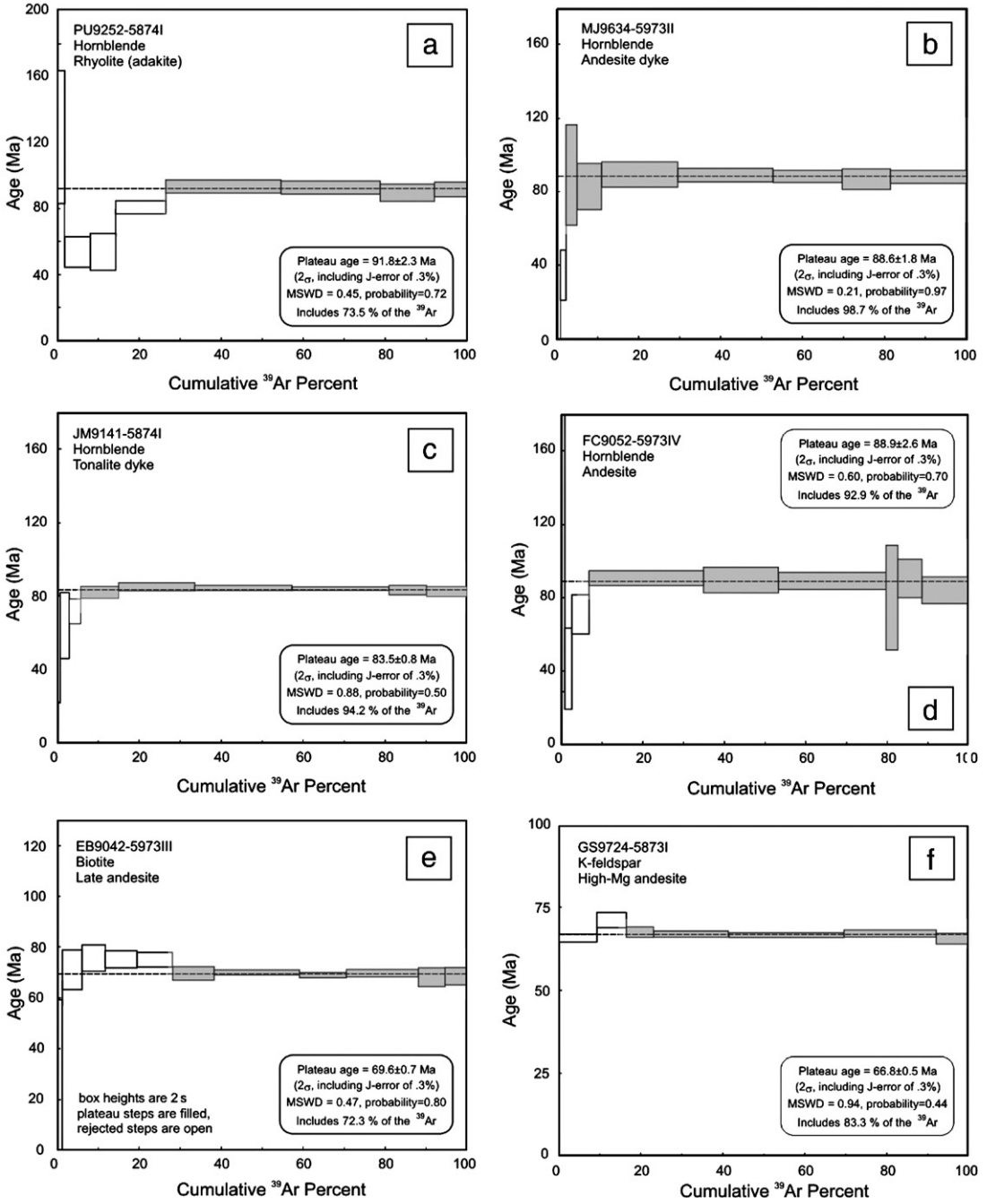


Fig. 5. $^{40}Ar/^{39}Ar$ age spectra for hornblende, biotite and K-feldspar in andesite, rhyolite and tonalitic dyke. The plateau ages were calculated following techniques described in the Appendix 1. A summary of $^{40}Ar–^{39}Ar$ incremental heating experiments is in the Appendix 3. Errors are quoted at the 2σ (95% confidence) level and are propagated from all sources except mass spectrometer sensitivity and age of the flux monitor.

5.3. Interpretation

The U–Pb and $^{40}Ar/^{39}Ar$ ages for rocks of the upper volcanic sequence of the Tireo Fm in this study can be divided in two broad groups (Fig. 6a): (93–83 Ma) Turonian–Santonian and (70–67 Ma) Maastrichtian ages. The andesitic to rhyolitic volcanic rocks of the upper sequence and related tonalite subvolcanic dikes, belong to the Turonian–Santonian main group of ages. The Turonian U–Pb age of the crystallization of the PU9024 adakitic

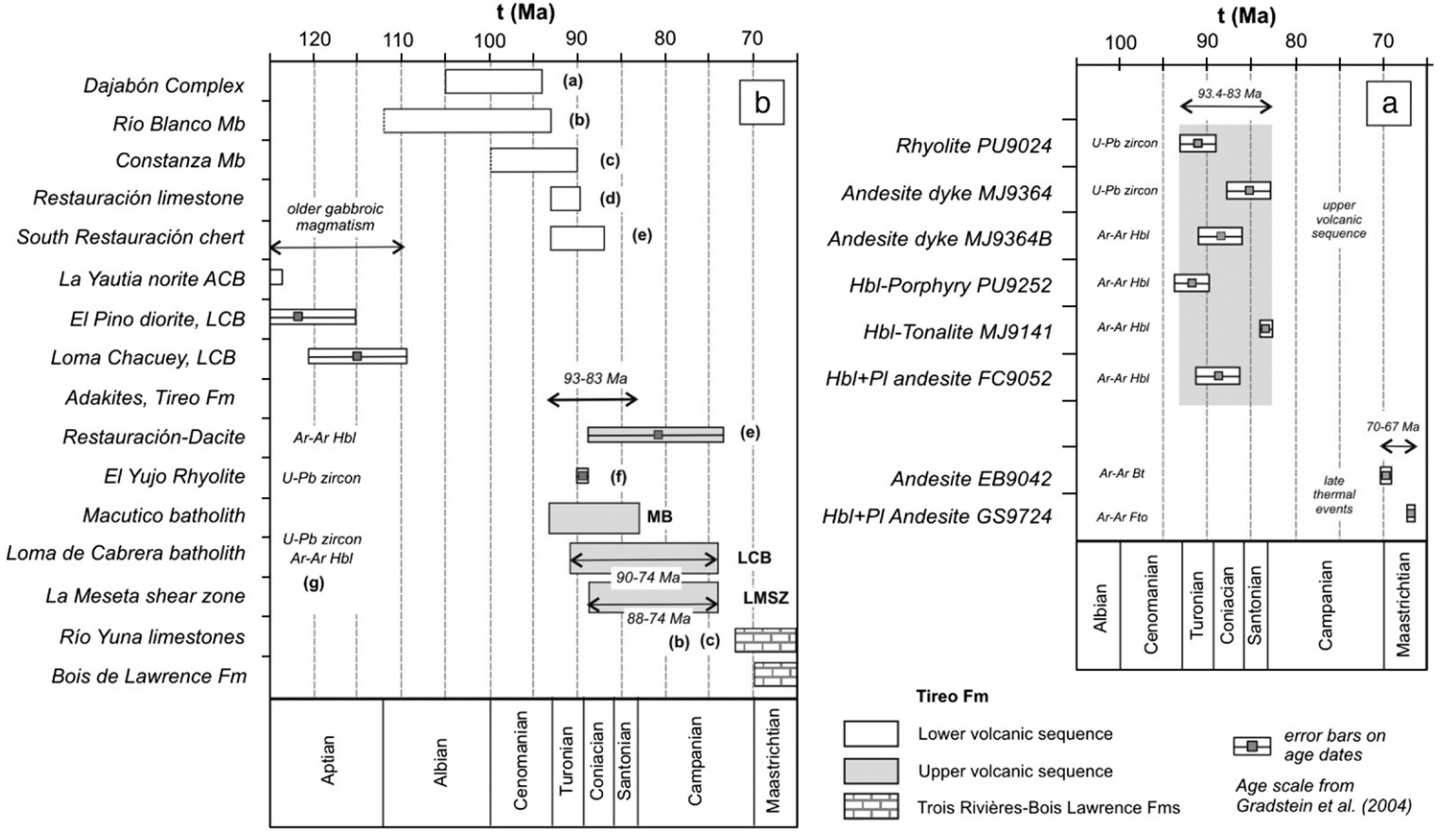


Fig. 6. (a) Summary of U–Pb and $^{40}Ar/^{39}Ar$ geochronological results in the upper volcanic sequence of the Tireo Fm; (b) Summary of paleontological and geochronological ages for the lower and upper volcanic sequence, older gabbroic magmatism, Loma de Cabrera (LCB) and Macutico (MB) batholiths and La Meseta shear zone amphibolites (LMSZ). Sources; (a) Albian to Upper Cenomanian (Montgomery et al., 1999); (b) Albian–Cenomanian (Gómez Sáinz, 2000); (c) Cenomanian–Turonian (Bowin, 1975); (d) Turonian Lewis et al. (1991, 2002); (e) Turonian to Coniacian (Lewis et al., 1991); (f) 89.0±0.9 Ma (Escuder Viruete et al., 2004); (g) (Contreras et al., 2004; Escuder Viruete et al., 2006a). Rectangles are the error bars (in 2σ).

rhyolite is equivalent to the Ar–Ar hornblende cooling age of the PU9252 adakitic rhyodacite, which is consistent with the field data. Also, these ages are similar to the U–Pb zircon age of 89.0±0.9 Ma (Turonian–Coniacian boundary) obtained for the lowermost rhyolite flows of the upper sequence in Jarabacoa area (Fig. 6a), and overlap within analytical error of the Ar–Ar hornblende cooling age of the FC9052 and MJ9364B arc-related andesite dikes. Therefore, the similarity in ages and subduction-related geochemistry (see below) support the integration of the Dajabón Complex in the Tireo Fm. These arguments also implies a genetic link between felsic rocks (adakites) of the upper volcanic sequence and the Hbl+Pl tonalite dykes intruded in the Tireo Fm. The Maastrichtian group of ages is related to the volumetrically minor late volcanism that appears below the limestones of the Late Maastrichtian Bois de Lawrence Fm. As shown in Fig. 6b, the upper volcanic sequence (93–83 Ma) is younger in age than the Constanza Mb (Cenomanian–Turonian) and the Restauración limestones (Turonian), stratigraphically located over the lower volcanic sequence. These results are also consistent with the Albian to Upper Cenomanian age of the lower volcanic sequence, obtain from microfossils by Montgomery et al. (1999) and Gómez Sáinz (2000). By other hand, the felsic volcanism of the upper volcanic sequence was coeval with the emplacement of the Hbl-bearing tonalite magmas in the Macutico (92–83 Ma) and Loma de Cabrera (90–74 Ma; Escuder Viruete et al., 2006a) batholiths, which is the extrusive equivalent.

6. Geochemistry

6.1. Chemical changes due to alteration and metamorphism

The purpose of this section is to distinguish different geochemical subduction-related mafic and felsic volcanic groups in the Tireo Fm; to show that there are petrogenetic relationships between these groups of rocks, particularly in the upper volcanic sequence; and to interpret the tectonic setting in which they formed. Representative geochemical data are reported in Table 1. Details of analytical techniques are in the Appendix 1. Tireo Fm rocks have been variably altered, deformed and metamorphosed to prenhite–pumpellite and lower greenschist facies. Consequently changes of the bulk-rock chemistry are expected as a consequence of selected mobility of relevant elements during alteration and/or metamorphism. Nevertheless, the concentrations of the high field-strength elements (HFSE) Y, Zr, Hf, Ti, Nb and Ta, the rare earth elements (REE), the transition elements V, Cr, Ni and Sc, and Th are generally unchanged under a wide range of metamorphic conditions, including seafloor alteration at low to moderate water/rock ratios (Bienvenu et al., 1990). Therefore, the discussion on petrogenesis and tectonic setting of the volcanic rocks will be based mostly on the REE and HFSE geochemistry, as it can be assumed that they were not significantly affected by alteration or metamorphism at the whole-rock scale.

6.2. Geochemical characteristics of mafic rocks

The geochemical characterization of mafic rocks is based in samples interpreted to best represent liquid compositions. The massive aphyric basaltic flows and the syn-volcanic basaltic or dolerite dykes, provide the best estimates as they do not commonly contain abundant phenocrysts. 15 cm-size, homogeneous aphyric clast of basalt and andesite in volcanic breccias are also interpreted represent a liquid composition. Dolerites and microgabbros have very similar trace element patterns to the mafic volcanic rocks, suggesting that the possible accumulated minerals have preserved the relative trace element abundances characteristic of the magmas from which they were derived.

The sampled volcanic rocks of the Tireo Fm range in composition from basalts, containing up to 15 wt.% MgO in some high-Mg rocks, to andesite, dacite and rhyolite (Table 1). For similar degrees of fractionation (i.e., Mg#), samples also reveal considerable variation in both the abundance of major and trace elements, trace element ratios and the patterns on primitive mantle-normalized extended-REE plots (Figs. 7–11). On the basis of these variations, mafic volcanic rocks of the Tireo Fm can be grouped into three geochemical groups: tholeiitic basalt-andesite suite; low-Ti, high-Mg andesites; and Nb-enriched basalts and andesites. Niobium-enriched basalts and andesites are defined on the basis of their high absolute Nb contents (>7 ppm), and having higher $(Nb/Th)_N$ and $(Nb/La)_N$ ratios than the majority of modern oceanic island arc basalts and andesites, plotting above the diagonal dashed line on Fig. 7 (Polat and Kerrich, 2001).

6.2.1. Tholeiitic basalt-andesite suite

The tholeiitic basalt-andesite suite is probably represented by the main amount of the poorly stratified lithic and vitric tuffs of the lower volcanic sequence, and certainly by the minor interbedded massive flows, monogenetic autoclastic breccias and syn-volcanic dykes (Table 1). These rocks range from unfractionated to quite fractionated compositions (Mg#=64–41). As a suite, the basalts and andesites define calc-alkaline trends of smoothly decreasing TiO_2, Fe_2O_3, Cr and Ni with increasing fractionation as monitored by MgO (Fig. 8),

Table 1
Whole-rock geochemical data for Tireo Formation

Group	IAT	IAT	IAT	IAT	IAT	HMA	HMA	HMA	HMA	HMA	HMA	HMA	NEBAI	NEBAI	NEBAI	NEBAII	NEBAII	NEBAII
Sheet	5874II	5873I	5873I	5974II	–	5973I	5974II	5973I	5974III	5974III	5974III	5973IV	6072II	6072I	5874I	6072I	6072II	5973IV
Unit	LVS	LVS	LVS	LVS	LVS	UVS	UVS	UVS	UVS	UVS	UVS	UVS	UVS	UVS	UVS	UVS	UVS	UVS
Rock	BAS	BAS	BAND	AND	BAS	BAND	BAND	BAND	BAS	BAND	AND	AND	DAC	BAND	AND	BAS	BAS	BAND
Sample	FC9068B	IGME6C	IGME7A	MJ9068	JE9901	MJ9208	FC9101	MJ9134	JE9013	JE9012	JE9010	FC9054	HH8003	AG8306	JM9141	AG8312	HH8006	FC9026
SiO_2	47.89	48.13	52.85	55.88	49.20	53.28	53.25	52.87	51.85	51.71	57.93	57.39	63.86	54.35	61.82	51.50	49.38	53.98
TiO_2	1.05	0.79	0.82	0.74	2.20	0.17	0.31	0.26	0.23	0.23	0.58	0.41	1.10	1.35	0.61	0.91	1.10	1.07
Al_2O_3	16.89	12.94	12.42	16.75	13.10	8.00	14.26	14.14	13.82	15.21	17.05	13.94	13.77	14.29	16.62	14.25	14.74	15.64
Fe_2O_3	9.04	10.48	9.73	8.92	15.10	11.79	10.08	10.79	11.44	9.59	5.28	9.25	5.94	10.84	4.95	9.60	11.25	10.16
MgO	8.24	9.14	7.09	3.11	4.60	13.90	7.68	8.00	8.09	6.39	4.87	5.55	3.36	5.37	1.72	8.82	8.28	5.11
CaO	11.21	11.02	10.60	5.33	9.10	8.95	10.10	8.27	11.23	11.75	6.04	4.05	3.86	4.82	2.01	9.04	10.29	9.65
Na_2O	2.82	2.34	1.70	5.44	2.60	0.71	2.95	3.20	1.53	1.24	4.02	4.32	4.00	3.84	5.67	2.76	2.91	1.84
K_2O	0.17	0.04	0.12	0.38	0.20	0.08	0.12	0.06	0.10	0.06	1.38	0.28	0.38	0.39	5.53	0.14	0.10	0.32
P_2O_5	0.14	0.06	0.06	0.08	2.60	0.06	0.06	0.04	0.04	0.02	0.24	0.07	0.13	0.21	0.19	0.07	0.12	0.09
MnO	0.15	0.17	0.16	0.15	0.30	0.26	0.13	0.17	0.17	0.15	0.05	0.13	0.06	0.13	0.11	0.17	0.18	0.16
Cr_2O_3	0.03	–	–	0.01	0.01	0.14	0.07	0.03	0.05	0.03	0.05	0.04	0.02	–	0.01	–	0.07	0.03
LOI	2.00	4.90	4.20	2.70	0.96	2.50	0.70	1.80	1.40	3.40	2.6	4.50	3.20	4.66	0.70	2.59	1.30	1.20
SUM	99.88	100.00	99.75	99.88	99.97	99.84	99.71	99.66	99.88	99.88	99.8	99.88	99.68	100.25	99.94	99.85	99.72	99.28
Mg#	64	63	59	41	38	70	60	59	58	57	65	54	53	50	41	65	59	50
Cr	212	527	386	34	14	978	465	212	369	219	405	274	30	34	82	490	473	178
Ni	56.2	201	141	6.6	26	186	24.1	47	19.6	39.4	120	89	22	75	5.6	177	133	57
Co	45.2	50.5	40.0	20.3	41	61.8	35.4	47.7	45	39	16	34	19	37	9.4	49	43	31.9
Sc	36	43.0	38.2	41	–	39	33	42	41	39	23	31	21.1	31	9	30	50.1	37
V	193	267	280	313	360	181	123	220	231	179	150	207	–	265	106	228	–	296
Rb	4.6	–	–	3.9	2	1.3	1.2	0.9	1.7	2.1	32	3.3	20	4	35.4	3	47	8.3
Ba	75	20	39	125	24	18	135	144	97	55	812	270	104	145	474	84	54	166
Th	0.3	0.5	0.5	0.3	0.8	0.2	0.8	0.6	<.1	0.3	1.8	0.6	2.8	1.8	1.9	1.6	–	0.9
U	<.1	0.5	0.5	0.2	0.2	<.1	0.2	0.2	<.1	0.1	0.5	0.4	0.2	0.6	0.7	0.4	–	0.5
Nb	2.0	0.6	0.4	0.8	5.1	0.25	2.2	1.1	0.2	0.9	3.7	2.6	5	12	10.9	8	5.2	7.7
La	4	2.80	2.60	2.9	10	1.2	3.9	3	1.8	2.2	7.13	4.2	16.4	17	13.5	11	–	8.1
Ce	11.1	7.5	7.0	8.4	24.3	2.8	7.0	5.9	2.9	3.8	12.7	9.0	34.0	39	28.1	23.0	–	18.0
Pb	0.4	2.1	3.0	0.2	0.1	<.1	0.2	0.5	0.2	<.1	5.6	0.6	–	2	3.9	6	–	0.9
Pr	1.73	–	—	1.28	3.8	0.43	0.94	0.74	0.5	0.54	1.5	1.29	–	4.95	3.45	2.9	–	2.33
Sr	270.5	75	188	143.7	130.0	9.7	149.5	217.3	193.3	109.9	811	263.4	225.0	117.0	134.5	274.0	131.0	329.4
Nd	9.9	5.0	5.0	7.3	17.5	2.6	4.7	3.6	2.5	3.1	–	6	19	21	14.6	12	–	10.7
Sm	3	1.5	1.5	2.1	4.3	0.7	1.1	0.9	0.7	0.8	–	1.6	4.3	4.8	3.2	2.8	–	2.8
Zr	84.4	32	39	54.7	134	13.1	23.7	17.1	5.5	15.1	89.8	38.9	109	95	114.1	69	35	63.2
Hf	2.4	1.0	0.9	2	3.8	<.5	0.8	0.6	<.5	0.5	2.8	1.4	4	2.7	3.1	1.9	–	1.9
Eu	1.24	0.6	0.6	0.75	1.7	0.2	0.55	0.37	0.33	0.38	0.42	0.55	1.4	1.65	1.07	0.99	–	1.11
Gd	3.91	–	–	3.13	5.9	0.82	1.66	0.9	0.84	0.84	1.2	1.78	–	4.3	2.91	2.6	–	2.56

Tb	0.74	0.5	0.5	0.71	1.1	0.13	0.3	0.13	0.15	0.17	0.18	0.31	0.6	0.8	0.54	0.5	–	0.59
Dy	4.24	–	–	3.64	6.5	0.71	2.08	0.79	0.87	1.03	1.2	1.83	–	4.1	3.19	2.5	–	2.41
Y	26.2	14.0	15.0	23.2	35.2	4.1	10.5	4.7	5.4	6.5	5.2	10.7	20	22	19.4	14	20	12.2
Ho	0.88	–	–	0.79	1.3	0.13	0.44	0.15	0.19	0.22	0.19	0.37	–	0.8	0.62	0.5	–	0.59
Er	2.73	–	–	2.46	3.8	0.45	1.25	0.51	0.57	0.6	0.48	1.08	–	2.1	1.93	1.4	–	1.29
Tm	0.4	–	–	0.35	0.6	0.07	0.15	0.08	0.09	0.1	0.08	0.16	–	0.33	0.31	0.19	–	0.3
Yb	2.48	1.6	1.7	2.29	3.9	0.39	1.17	0.51	0.61	0.65	0.53	1.01	1.8	1.8	1.94	1.1	–	1.27
Lu	0.41	0.2	0.3	0.37	0.6	0.08	0.2	0.08	0.1	0.12	0.08	0.17	0.28	0.24	0.36	0.16	–	0.3
$(La/Yb)_N$	1.16	1.26	1.10	0.91	1.84	2.21	2.39	4.22	2.12	2.43	6.9	2.98	6.54	6.78	4.99	7.18	–	4.58
$(Sm/Yb)_N$	1.34	1.04	0.98	1.02	1.22	1.99	1.04	1.96	1.27	1.37	–	1.76	2.65	2.96	1.83	2.83	–	2.45
$(Zr/Sm)_N$	1.12	0.85	1.03	1.03	1.24	0.74	0.85	0.75	0.31	0.75	–	0.96	1.00	0.78	1.41	0.98	–	0.89

Group	NEBAII	NEBAII	DR	DR	DR	DR	ADAK	ADAK	ADAK	ADAK	ADAK	ADAK	INTR	INTR	INTR
Sheet	5873I	5873I	5973IV	6072II	6073I	6072IV	5873I	5874I	5873I	6073II	5874I	5874II	5974II	5873I	5874II
Unit	UVS	UVS	UVS	UVS	UVS	UVS	UVS	UVS	UVS	UVS	UVS	UVS	UVS	UVS	UVS
Rock	DAC	DAC	DAC	DAC	RHY	RHY	RHY	RHY	DAC	DAC	RHY	RHY	TON	TON	TON
Sample	GS9320	BGS9320	FC9052	HH8005	02J93	AG8507	GS9891	PU9024	GS9032	2JE115	PU9252	FC9052L	FC9094	GS9080	FC 9070
SiO_2	63.80	63.00	62.46	62.16	70.50	83.38	68.11	74.99	64.21	67.32	74.20	76.25	66.68	68.79	74.16
TiO_2	0.89	0.87	0.47	0.52	0.65	0.14	0.24	0.21	0.29	0.36	0.30	0.19	0.21	0.50	0.17
Al_2O_3	14.01	14.06	15.43	15.47	13.00	9.08	12.55	12.84	12.13	13.75	12.08	11.55	11.73	13.24	13.02
Fe_2O_3	5.56	5.45	6.62	7.39	5.68	1.44	5.00	2.16	7.20	6.50	3.67	1.56	6.85	5.26	2.52
MgO	2.88	2.88	3.22	2.15	0.88	0.05	4.60	1.79	4.03	3.22	1.01	0.37	3.39	1.60	0.51
CaO	2.98	3.09	6.49	4.20	3.10	0.10	0.54	0.92	3.94	1.85	2.69	2.69	3.68	4.46	1.36
Na_2O	4.42	4.08	3.30	2.34	5.20	4.64	5.11	2.86	4.10	1.86	3.33	5.46	2.69	3.55	4.72
K_2O	2.01	2.40	0.28	1.73	0.12	0.49	0.33	1.85	0.77	2.06	0.99	0.08	0.41	0.67	1.43
P_2O_5	0.16	0.15	0.18	0.03	0.10	0.01	0.07	0.05	0.07	0.09	0.06	0.04	0.05	0.09	0.03
MnO	0.10	0.09	0.09	0.04	0.06	0.01	0.08	0.04	0.10	0.09	0.04	0.02	0.09	0.11	0.04
Cr_2O_3	0.02	0.01	0.02	0.02	0.01	–	0.02	0.02	0.02	0.02	0.05	0.02	0.03	0.02	0.01
LOI	2.60	3.40	1.30	3.70	0.55	0.80	2.90	2.20	2.70	2.80	1.40	1.60	3.40	1.30	1.50
SUM	99.88	99.88	99.88	99.75	99.85	100.14	99.88	99.93	99.88	99.92	99.82	99.88	99.21	99.59	99.47
Mg#[(1)]	51	51	49	37	23	6	65	62	53	50	35	32	49	38	29
Cr	116	89	144	13	108	10	130	109	109	151	308	116	219	103	41
Ni	12	16	49	8	16	8	49	3.2	32	22.6	15.1	15.6	28.4	4.2	5.3
Co	18.3	15.7	18.6	14	5	0.5	16.6	2.1	24.2	16.2	9	1.3	20.3	12.2	2.7
Sc	17	17	19	18.9	–	6	17	7	25	22	12	12	23	19	6
V	151	140	146	–	72	7	89	15	152	129	100	4	138	94	15
Rb	27.7	32.6	5.5	18	2	8	3.7	26.7	8.5	40.6	11.6	1.3	9	9.2	20.9
Ba	558	637	545	191	159	129	182	595	340	497	468	36	216	379	646
Th	4.6	3.9	2.7	1.1	2.3	2.2	1.5	3.8	2.0	1.4	3.5	1.3	1.6	2.4	4.1
U	1.2	1.1	1	0.2	0.83	0.7	0.7	1.1	0.8	0.6	0.9	0.6	0.7	0.5	1.2
Nb	15.8	14.5	9.6	5	6	8	2.2	6.1	5.1	5.5	3.2	7.2	3.6	8.6	4.2
La	21.1	19.7	16.1	6.6	8.9	6.6	11.1	13.7	9	12.6	8.1	11.7	10.7	11.7	15.3

(continued on next page)

Table 1 (*continued*)

Group	NEBAII	NEBAII	DR	DR	DR	DR	ADAK	ADAK	ADAK	ADAK	ADAK	ADAK	INTR	INTR	INTR
Ce	44.6	41.9	29.5	16.0	16.5	13.0	22.4	26.8	15.9	23.0	15.2	22.3	20.6	26.0	28.8
Pb	1.7	1.6	0.2	–	10	1	1	0.5	2.3	1	2	0.1	0.5	0.4	0.6
Pr	5.53	5.03	3.15	–	2.64	1.74	2.57	3.35	1.72	2.88	1.62	3.09	2.69	3.37	3.31
Sr	378.9	492.2	600.4	231.0	130.0	52.0	122.2	164.9	188.1	233.5	344.2	107.4	293.1	338.6	289.1
Nd	24.6	23	13.6	10	11.7	7.3	11	14.4	7.6	13.5	6.2	14.9	11.8	15.6	13.3
Sm	4.3	4.2	2.5	2.1	2.2	1.6	2	2.9	1.6	2.6	1.3	3.8	2.1	3.4	2.7
Zr	138.9	125.2	103	37	108	107	65.1	104.8	59.1	76.1	111.8	124.3	62.9	116.5	100.1
Hf	4	3.8	2.6	2	3	3.1	2.1	2.9	1.6	2.5	2.9	3.5	1.7	3.4	3.2
Eu	1.36	1.2	0.85	1.1	0.88	0.32	0.47	0.82	0.5	0.66	0.45	0.73	0.61	0.92	0.66
Gd	4.22	3.78	1.9	–	3.13	1.4	1.83	2.34	1.27	2.4	1.46	5.11	1.84	3.08	2.24
Tb	0.62	0.64	0.3	0.2	0.54	0.3	0.28	0.35	0.21	0.25	0.23	0.85	0.22	0.53	0.35
Dy	2.76	2.76	1.59	–	3.2	1.7	1.38	1.78	0.98	1.49	1.22	5.23	1.11	2.63	1.52
Y	14.7	14	8.9	13	16	11	7.2	11.3	5.3	6.8	6.6	34.6	5.8	13.8	8.9
Ho	0.51	0.5	0.31	–	0.68	0.4	0.24	0.32	0.19	0.21	0.21	1.07	0.18	0.49	0.31
Er	1.38	1.34	0.89	–	1.95	1.3	0.74	1	0.46	0.7	0.65	3.2	0.51	1.36	0.81
Tm	0.2	0.2	0.12	–	0.28	0.22	0.1	0.13	0.07	0.11	0.09	0.47	0.08	0.19	0.14
Yb	1.25	1.24	0.88	1.5	1.9	1.4	0.73	0.99	0.46	0.81	0.61	2.93	0.48	1.24	0.93
Lu	0.19	0.2	0.14	0.2	0.27	0.22	0.12	0.16	0.08	0.11	0.1	0.45	0.09	0.2	0.14
$(La/Yb)_N$	12.11	11.40	13.13	3.16	3.36	3.38	10.91	9.93	14.04	11.16	9.53	2.87	16.00	6.77	11.81
$(Sm/Yb)_N$	3.82	3.76	3.15	1.55	1.29	1.27	3.04	3.25	3.86	3.56	2.37	1.44	4.86	3.04	3.22
$(Zr/Sm)_N$	1.28	1.18	1.63	0.70	1.95	2.65	1.29	1.43	1.46	1.16	3.41	1.30	1.19	1.36	1.47

Major oxides recalculated to an anhydrous basis. Total Fe as Fe_2O_3. [(1)]$Mg\# = 100 \times mol\ MgO/[mol\ MgO + mol\ FeO_{total}]$. $Nb/Nb^* = 0.3618 \times Nb/(Th \times La)^{0.5}$.

Rock Group: IAT, island arc tholeiites; HMA, high-Mg andesitas; NEBA, Nb-enriched basalts; DR, dacites and rhyolites; ADAK, adakites; INTR, tonalitic dykes.

Rock Unit: LVS, lower volcanic sequence; UVS, upper volcanic sequence.

Rock: BAS, basalt; BAND, basaltic andesite; AND, andesite; DAC, dacite; RHY, rhyolite; TON, Hbl-bearing tonalite.

Sheet: 5874II, Loma de Cabrera; 5873I , Restauración; 5874I, Dajabón; 5974II, Monción; 5974III, Santiago Rodríguez; 5973I, Diferencia; 5973IV, Jicomé; 6072II, Sabana Quéliz; 6072I, Constanza; 6072IV, Gajo del Monte; 6073I, La Vega; 6073II, Jarabacoa.

but they have relatively uniform Nb, Zr and Yb, with La/Yb<4 (1.2–1.6) more characteristic of tholeiitic fractionation trends (Jolly et al., 2001). The extended REE patterns (Fig. 9) are very similar to other Caribbean island arc tholeiites (Jolly et al., 1998; Escuder Viruete et al., 2006b) and at similar absolute abundances (HREE 3–7× primitive mantle). In particular, REE/HFSE ratios (e.g. La/Nb and Sm/Zr) are high in these basalts and andesites relative to N-MORB compositions, which is typical of IAT. They have slightly LREE-depleted to slightly LREE-enriched patterns ($[La/Yb]_N$=0.9–1.4; average 1.1), pronounced negative Nb anomaly (Nb/Nb*=0.2–0.7), slight negative Zr and positive Hf anomalies ($[Zr/Sm]_N$=0.9–1.2) and flat HREE. The TiO_2 content ranges between 0.7 and 1.1 wt.%.

6.2.2. Low-Ti, high-Mg andesites

The low-Ti, high-Mg andesites are represented by part of the interbedded mafic rocks in the upper volcanic sequence, and some syn-volcanic dykes of dolerite and microgabbro. These rocks extend to less fractionated compositions (Mg#=70–46) than the tholeiitic suite. The high-Mg andesites are characterized by anomalously high MgO (14.3–4.8 wt.%), Cr (978–226 ppm) and Ni (186–20 ppm) contents for a basalt-andesite range of SiO_2. They plot consistently above the divide between the normal arc field and magnesian andesites of McCarron and Smellie (1998) (Fig. 8). The La/Yb<4 (2.4–4.1) and the extended-REE patterns of these rocks are similar to the tholeiitic suite, with a pronounced negative Nb anomaly (Fig. 9), but the absolute abundances are lower (HREE 1–6× primitive mantle), the negative Zr and Hf anomalies are greater ($[Zr/Sm]_N$=0.3–1.1; average 0,78), and there is consistent LREE enrichment ($[La/Yb]_N$=1.7–4.2; average 2.7). The TiO_2 content range between 0.2 and 0.6 wt.% and is considerably lower than that of tholeiites at a given value of MgO. Compared to "normal" IAT, high-Mg andesites also trend to greater Th and Ce at higher MgO but to lower Nb, and have near-flat trends for Zr, Y, and Yb with MgO (Fig. 8). The lower TiO_2 and HREE contents (particularly Yb), and negative Zr and Hf anomalies suggest that the source for these rocks was more depleted than for tholeiites. Also, the highly magnesian composition of the andesites and basalts demands high melting temperatures and relatively rapid transit of the magmas through the crust (Yogodzinski et al., 2001).

6.2.3. Nb-enriched basalts and andesites

Niobium-enriched basalts to andesites have been identified as flows and dykes in the upper volcanic sequence, where they coexist with related high-Ti (some

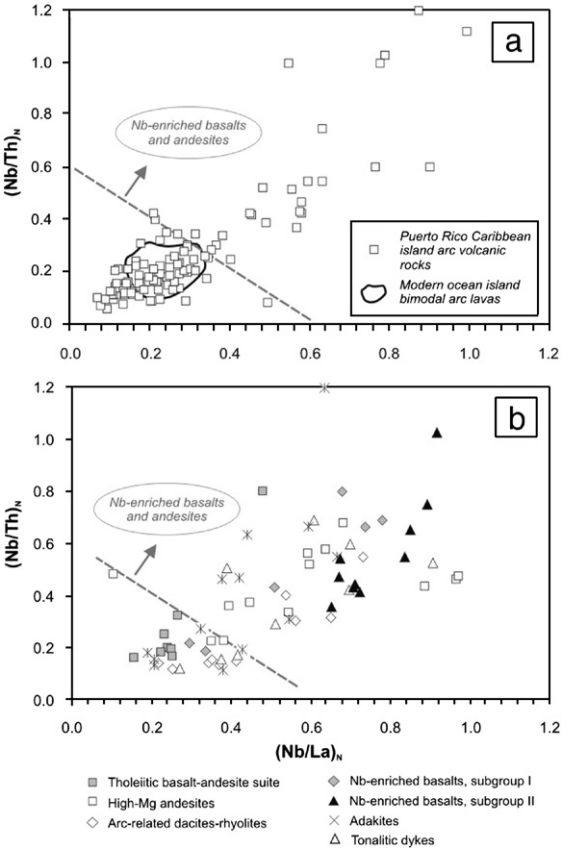


Fig. 7. Variation diagram of $(Nb/La)_{pm}$ *vs* $(Nb/Th)_{pm}$. (a) Modern oceanic island arc volcanic rocks and Puerto Rico Caribbean island arc volcanic rocks (Jolly et al., 1998, 2001, 2006) plot below the diagonal dashed line. (b) Mafic rocks from the Tireo Fm with high Nb contents (>7 ppm) and plotting above the dashed line are designated as Nb-enriched (Polat and Kerrich, 2001).

also high-Mg), Nb-rich dacites. Collectively, Nb ranges from 5 to 16 ppm (Fig. 8), compared to <2 ppm in most basalts of intra-oceanic arcs (Martin et al., 2005). Compositionally, they vary in the range 48–66 wt.% SiO_2 and 8.8–3.4 wt.% MgO (Table 1). Against MgO, these rocks show a decrease of Fe_2O_{3T}, TiO_2, CaO, alkalis, V, Cr and Ni; and an increase in SiO_2, Nb and Zr for decreasing MgO (not all shown in Fig. 8). Compositionally, these rocks are similar in many respects to the Nb-enriched basalts described by Defant et al. (1991), Maury et al. (1996) and Sajona et al. (1996). Compared to high-Mg andesites, this group trend to greater TiO_2, Nb, Zr, Th, Y and Yb with MgO and also have major $(La/Yb)_N$ and $(Sm/Yb)_N$ ratios. However, the TiO_2, Nb, Zr, Y, Yb–MgO variations and extended-REE pattern, shows two slightly distinct trends of Nb-enriched basalts and andesites (Fig. 10). The subgroup I show REE patterns that are slightly LREE-enriched ($[La/Nd]_N$=1.8–2.2) and

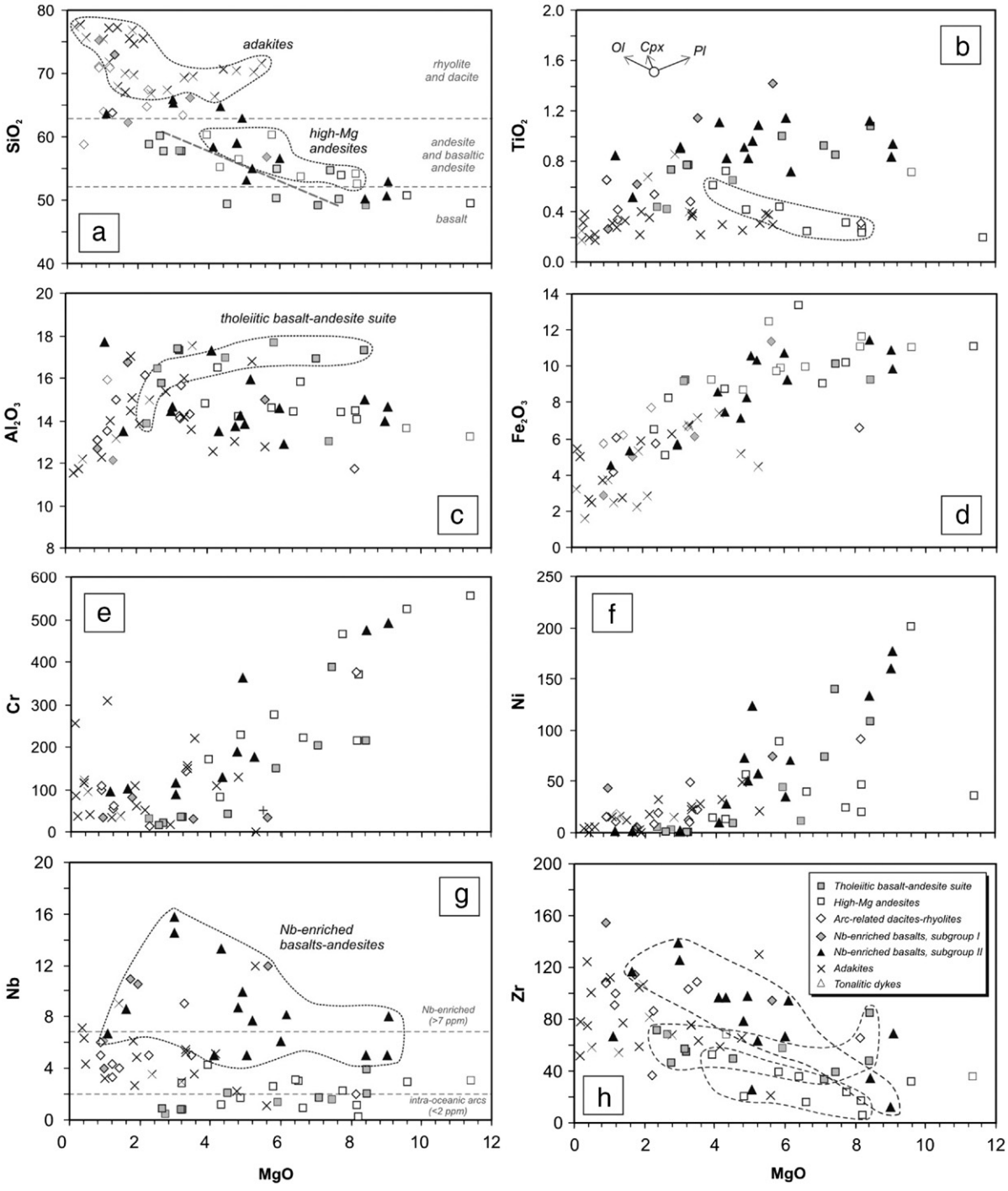


Fig. 8. Plots of selected major and trace elements against MgO of the Tireo Fm.

HREE (and Y)-depleted ($[Sm/Yb]_N$=1.8–2.9), for low absolute abundances (HREE 4–7×primitive mantle). Moreover, they have slightly negative Nb (0.3<Nb/Nb*<0.8) and Zr ($[Zr/Sm]_N$=0.8–1.5), but pronounced negative Ti anomalies. The TiO_2 content ranges between 0.6 and 1.4 wt.%. The extended-REE patterns of the subgroup II and absolute abundances (HREE 2–7×primitive mantle) are similar to subgroup I, but there is

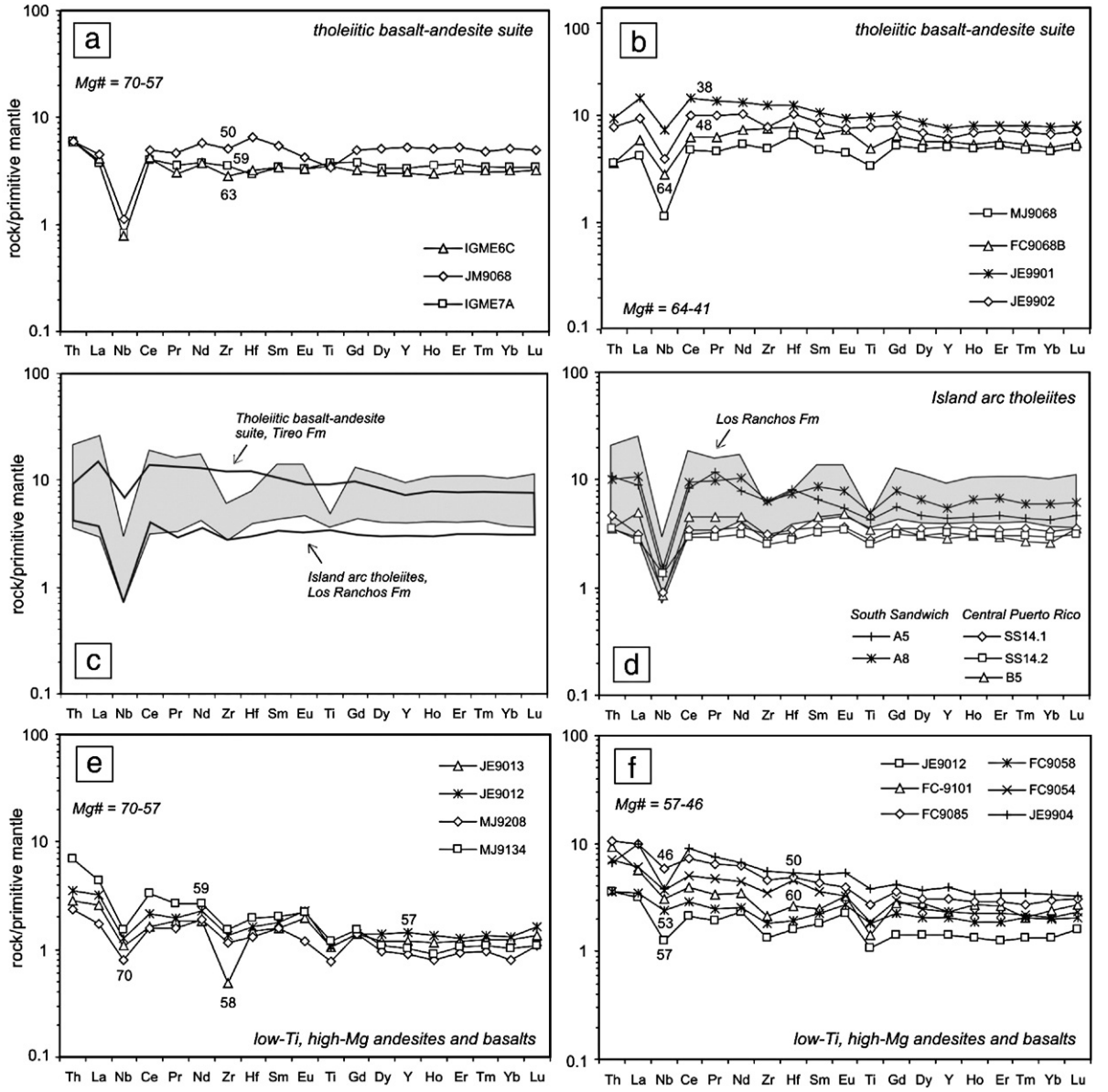


Fig. 9. Primitive mantle-normalized extended-REE diagrams of the Tireo Fm: (a, b) tholeiitic basalt-andesite suite of the lower volcanic sequence; (c) island arc tholeiites of the Los Ranchos Fm (Escuder Viruete et al., 2006b); (d) island arc tholeiites from the volcanic phase I, Central Puerto Rico (Jolly et al., 1998, 2001) and from Thule island of the South Sandwich arc (Leat et al., 2004); (e, f) high-Mg andesites and basalts of the upper volcanic sequence. Normalizing values are from Sun and McDonough (1989).

consistent more LREE-enrichment ($[La/Nd]_N$=1.7–2.3), with slightly negative Nb (0.7>Nb/Y>1.0) and marked depletion in HREE ($[Sm/Yb]_N$=2.4–4.1). The TiO_2 contents range between 0.7 and 1.2 wt.%. These features suggest that the mantle source for subgroup II was more enriched than subgroup I. Also, the sources for Nb-enriched groups were more enriched than for the tholeiitic suite and high-Mg andesites.

6.3. Geochemical characteristics of felsic rocks

The felsic rocks of the Tireo Fm includes the volcanic rocks of the upper sequence, the related intrusive subvolcanic domes, and the intrusive Hbl-bearing tonalite dykes. These rocks can be grouped into two geochemical groups, although probably there are transitional compositions between them: (1) dacites-rhyolites and (2) adakites.

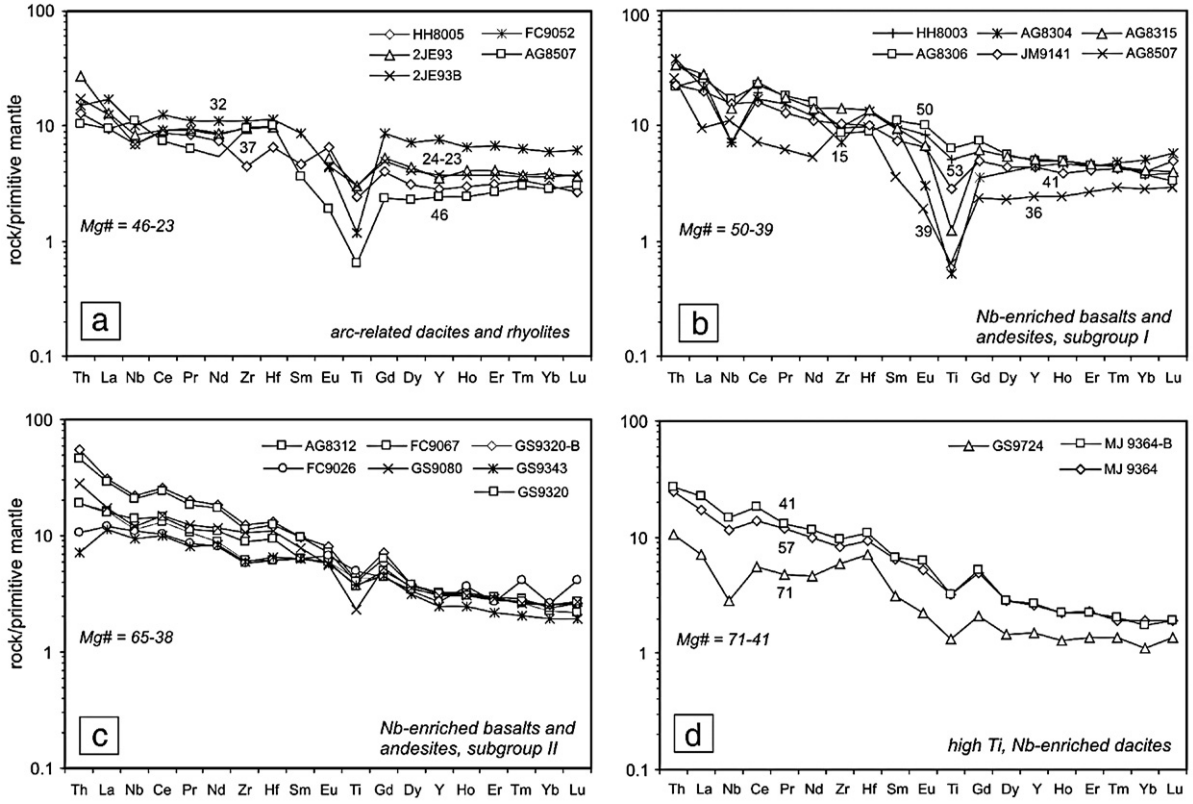


Fig. 10. Primitive mantle-normalized extended-REE diagrams of the (a) arc-related dacites and rhyolites; (b, c) subgroups I and II of Nb-enriched basalts and andesites; and (d) related high-Ti, Nb-enriched dacites of the upper volcanic sequence.

6.3.1. Dacites and rhyolites

Dacites and rhyolites have Mg# from 37 to 23, and form a low-Ti trend with high-Mg andesites in the Fig. 8. All these felsic rocks are low in K_2O (<0.7 wt.% in rhyolites), TiO_2 (0.2–0.6 wt.%), P_2O_5 (<0.1 wt.%) and Zr, relative to typical calc-alkaline felsic rocks. Rhyolites have $(La/Yb)_N$=2.8–6.5 and, in general, lack the moderate to strong LREE enrichment typical of the calc-alkaline felsic rocks and thus are interpreted to have a tholeiitic transitional to calc-alkaline affinity. Dacites and rhyolites have REE patterns (Fig. 11) that are flat to slightly LREE-enriched ($[La/Nd]_N$=1.5–1.7) or HREE (and Y)-depleted ($[Sm/Yb]_N$=1.3–1.6) for low absolute abundances (HREE 3–5×primitive mantle). Moreover, they have slightly negative Nb (0.4<Nb/Nb*<0.7) and, in occasions, Zr anomalies. The TiO_2 contents range between 0.5 and 0.7 wt.%. High-SiO_2 (>70 wt.% SiO_2), low-K, felsic volcanism in intra-oceanic arc systems is generally interpreted as the products of deep partial melting, as opposed to fractionation, of mafic rocks (Tamura and Tatsumi, 2002). Processes of dehydration melting of underplated lower crust arc material can generate the felsic magmatism in a developing intra-oceanic arc, as has been proposed for the Kermadec (Smith et al., 2003) and Caribbean arcs (Escuder Viruete et al., 2006b).

6.3.2. Adakites

Compositionally, adakites are Al-enriched dacite to rhyolite and were found in the upper volcanic sequence of all studied areas (Fig. 3). In addition of Al_2O_3 contents of 12–18 wt.%, the adakites are distinctive in: (1) high La but low Yb contents resulting in extremely fractionated REE (Y=5.3–14.7 ppm; $(La/Yb)_N$=11–32); (2) relatively high TiO_2 (0.3–0.9 wt.%), Fe_2O_3, MgO (0.4–5.3 wt.%), Cr (116–308 ppm) and Ni (15–49 ppm) contents in general; (3) minor Eu anomalies; and (4) pronounced troughs at Nb, Ti, Sc and V (Nb/Nb*=0.2–0.9; Fig. 11, Table 1). They also possess variable Nb/Ta (10.7–17.7) and Zr/Hf (30.4–42.1) ratios, and both positive and negative fractionation of Zr relative to Sm. The Hbl-bearing tonalite dykes intrusive in the Tireo Fm have a very similar extended-REE pattern to adakites, which suggest than they are the intrusive equivalents.

7. Discussion

7.1. Mantle and slab contributions in the mafic volcanic rocks

In arc magmas, the concentration of a given element is determined by the partial melting and crystal fractionation history of a source containing both mantle-derived and slab-derived components, both of which may vary considerably in composition (Pearce and Peate, 1995). For the least fractionated mafic samples of each geochemical group of the Tireo Fm, the relative contribution of the each component can be evaluated using the method proposed by Pearce and Parkinson (1993). In all mafic types (Fig. 12), the slab contribution above the "baseline" connecting the mantle derived elements (HFSE and HREE) includes variable proportions of LILE, LREE y MREE elements, which were mobilized by aqueous fluids. Therefore, a first orden interpretation is that mafic volcanic rocks of the Tireo Fm were produced by variable degrees of melting by fluxing of a mantle source with subduction-related hydrous fluids. In the tholeiitic suite of the lower volcanic sequence, the HFSE and HREE form a trend subparallel to the N-MORB normalizing value and at similar absolute abundances (Fig. 12). Such a pattern suggest a similar degree of melting that MORB and does not require residual amphibole or minor phases in the source, or complex melt–residue interactions in the melting column. In the Nb-enriched basalts and high-Mg andesites, Y and HREEs have compositions subparallel to the *x*-axis, although at progressive lower absolute levels. This feature can be explained by an increasing in degree of melting relative to MORB, from rocks of the tholeiitic suite to Nb-enriched basalts to high-Mg andesites. However, variations in melting are not sufficient to explain the upward slope of the left side of the baseline for high-Mg andesites and Nb-enriched basalts of the upper sequence, indicating that other factors are responsible for relative enrichments of Nb, Zr, Hf and Ti in the mantle wedge. The enrichment of these elements is attributed to small degrees of melting with residual garnet (Pearce and Parkinson, 1993), to an ocean-island-basalt-like (plume) component (Stern, 2002), or to melting of the subducting slab in the eclogite to garnet amphibolite facies conditions (Defant and Drummond, 1990; Pearce and Peate, 1995; Sajona et al., 1996; Martin et al., 2005). In these cases, these elements may not be reliable indicators of the mantle

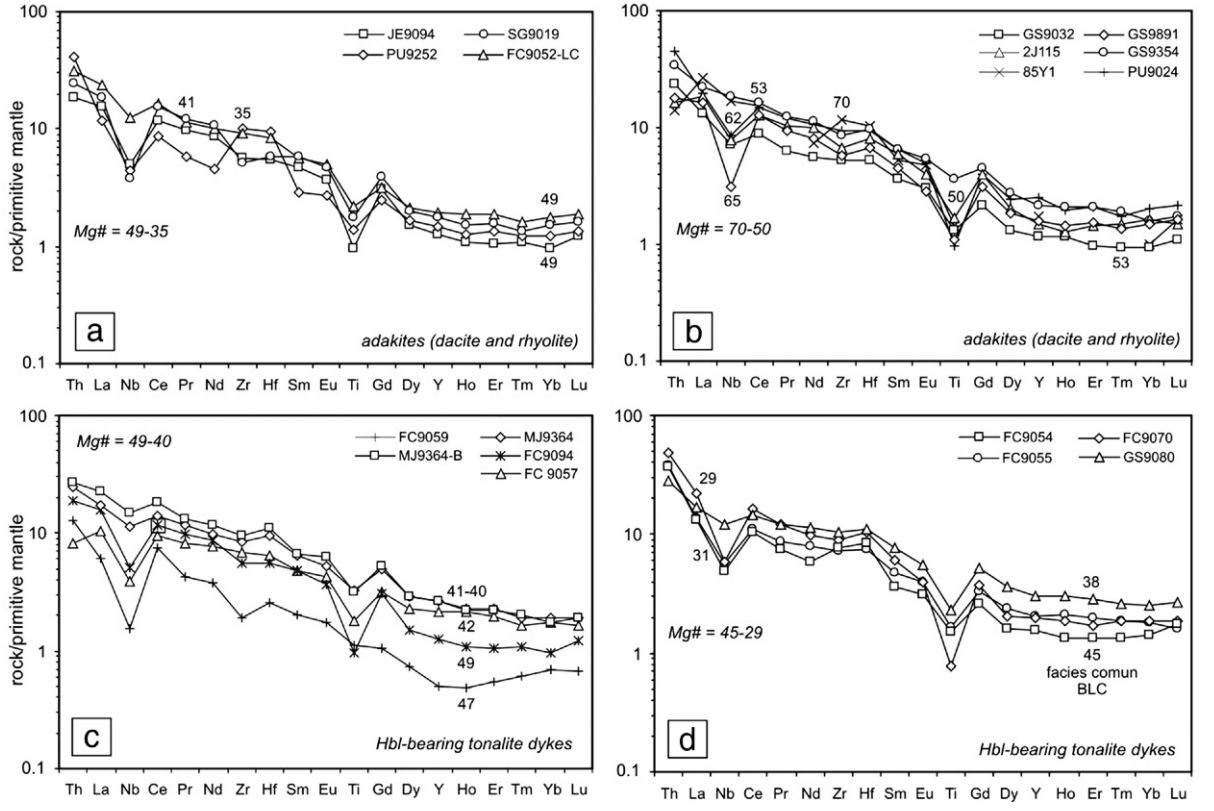


Fig. 11. Primitive mantle-normalized extended-REE diagrams of: (a, b) adakites; and (c, d) Hbl-bearing tonalite dykes intrusive in the Tireo Fm.

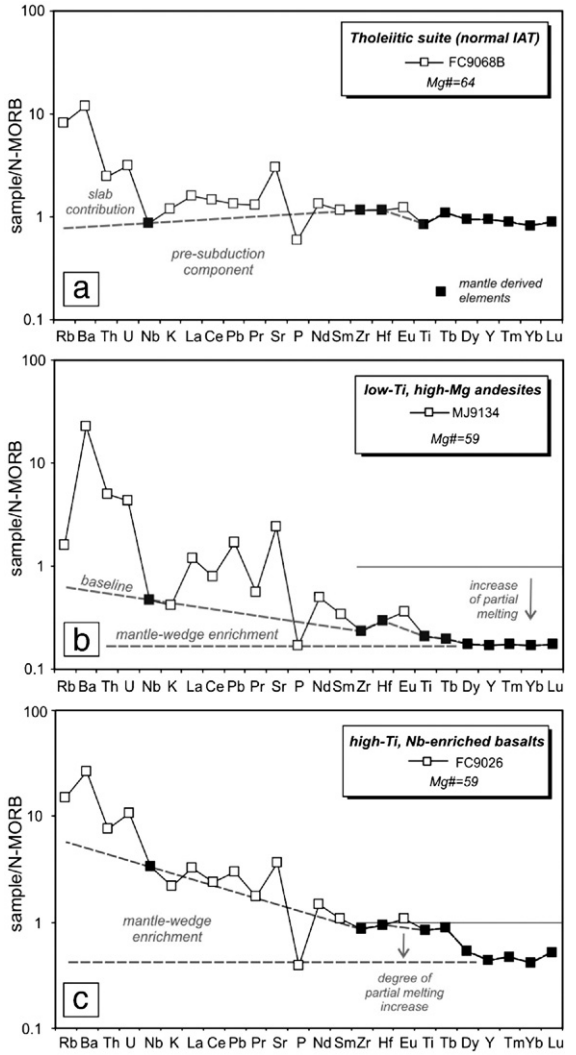


Fig. 12. MORB-normalized trace-element plot for low fractionated rocks of the different mafic geochemical groups defined in the Tireo Fm. Elements thought to be derived primarily from the mantle wedge are shown as black squares, whereas those which involve a significant subduction component are shown as white squares. The left side of the baseline indicates the extrapolated abundances in the mantle wedge of those elements mainly derived from the subducting slab. Normalizing values and orden of relative incompability with a fertile spinel-lherzolite mantle are taken from Pearce and Parkinson (1993). See text for discussion.

behaviour. Therefore, a change in the nature of the source region exists between the mafic rocks of the lower and upper volcanic sequences of the Tireo Fm.

7.2. Degree of partial melting and source enrichment

A trace-element plot of Nb and Yb normalized to 9.0 wt.% MgO ($Nb_{9.0}$ *vs* $Yb_{9.0}$; Fig. 13) allows the effects of partial melting to be separated from those of source depletion or enrichment (Pearce and Parkinson, 1993). To build this plot for Tireo Fm volcanics, samples with MgO < 5 wt.% have been removed and the fields of primitive IAT of the Los Ranchos Fm have been included (Escuder Viruete et al., 2006b). Although magmas at 9 wt.% MgO are not primary, they lie on the olivine-Cr spinel cotectic and are close to primary compositions for incompatible trace elements, which allow minimisation of the effects of fractional crystallization. Fig. 13 does support the existence of different mantle sources for mafic volcanics of the Tireo Fm, from slightly depleted and fertile MORB mantle (FMM) to primitive upper mantle (PUM) and more enriched. This diagram corroborates the low to moderate melting proportions (5–15% of FMM) required by tholeiitic rocks and subgroup I of Nb-enriched basalts, and high to very high (about 25–45%) for high-Mg andesites and subgroup II, with a clear separation of each mafic group into discrete melt populations. In Fig. 13, tholeiitic suite compositions fall between FMM and 5% source depletion melting trends, as well as Los Ranchos Fm IAT volcanics, which is consistent with the maximum of about of 3% of melt removed from the mantle during the depletion processes even in the most extremely depleted islands of the Tonga, Kermadec and South Sandwich arcs, with thin lithosphere and associated active back-arc basins (Pearce and Parkinson, 1993). High-Mg andesites and subgroup I of Nb-enriched basalts compositions plot above PUM melting trend since they can have a slab-related Nb enrichment. Also, the more enriched sources of the high-Ti, subgroup II of Nb-

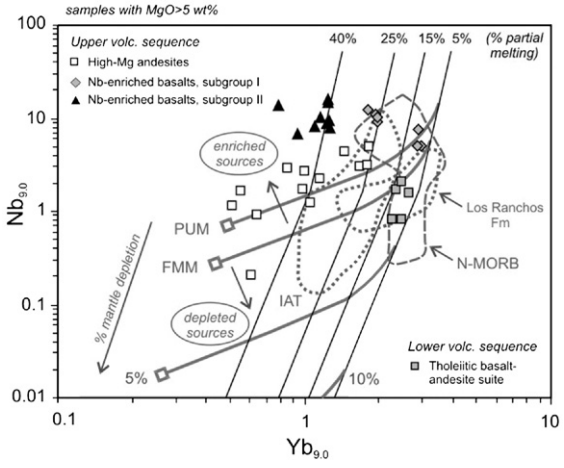


Fig. 13. Nb *vs* Yb plot, with trace element compositions normalized to MgO = 9 wt.%. Contours for partial melting and enrichment/depletion are after Pearce and Parkinson (1993). FMM, fertile MORB mantle; PUM, primitive upper mantle composition.

enriched basalts require the highest degrees of melting (30–40%).

7.3. Fractional crystallization versus mixing trends

Tireo Fm volcanic rocks exhibit a large compositional variation both within and between the defined geochemical groups. The basalt-andesite suite and high-Mg andesites have tholeiitic affinity; however, Nb-enriched basalts have (La/Yb)>4 values and show trends of decreasing Fe_2O_3 and Zr, with increasing fractionation more characteristic of a calc-alkaline fractionation trend (Fig. 8). Likewise, the incompatible element contents and ratios in the mafic volcanics exhibit significant variations from the exposed base upward, for example the lower sequence trend to slightly lower whereas the upper volcanic sequence trend to higher $(La/Yb)_N$ and $(Sm/Yb)_N$ ratios. As has been argued, possible mechanism to explain these variations include fractional crystallization and partial melting of heterogeneous source regions. Rocks from the Tireo Fm display wide ranges of Cr (1266-3 ppm) and Ni (244-1 ppm) contents and, for each group, there are good correlations between some elements as SiO_2, MgO, TiO_2, Y e Yb. These features, in combination with the variable anomalies in Ti, Nb and Eu with evolution, argue for some degree of fractional crystallization (or accumulation) of a Ti-bearing phase and plagioclase. However, fractional crystalization alone cannot explain the observed geochemical variations, particularly in $(Sm/Yb)_N$ and $(Zr/Sm)_N$ ratios, because these features are relatively insensitive to magmatic differentiation (Pearce and Peate, 1995). Thus, the differences in compositional trends can best be explained by derivation of tholeiitic suite, high-Mg andesites and Nb-enriched magmas from different mantle sources. In high-Mg andesites and Nb-enriched basalts, REE contents and $(La/Yb)_N$ ratios do not systematically covary with indices of fractionation such MgO or SiO_2 in a manner consistent with amphibole and magnetite crystal fractionation. In these groups, those basalts and andesites with the greatest LREE contents generally also possess high $(La/Yb)_N$ ratio, low Yb, deep Nb and Ti troughs, low Cr, Co and Ni contents, and pronounced depletion of Sc and V relative to REE. These are all compositional characteristics of adakites, yet these samples are too low in SiO_2, MgO, and Fe_2O_3 to be adakites. In summary, the volcanic rocks of the lower volcanic sequence of the Tireo Fm constitute an association of tholeiitic basalt-andesite, which is usually interpreted in terms of melting by fluxing of a mantle wedge with subduction-related hydrous fluids. The complex spectrum of basalt and andesite compositions of the upper volcanic sequence is interpreted in terms of some combination of calc-alkaline fractionation trends, with hybridization (metasomatism) of the source of the basalts and andesites by Al-rich adakite liquids. Such process is expressed by the spread of the samples along mixing trends between average MORB basalt and adakite compositions in Fig. 14.

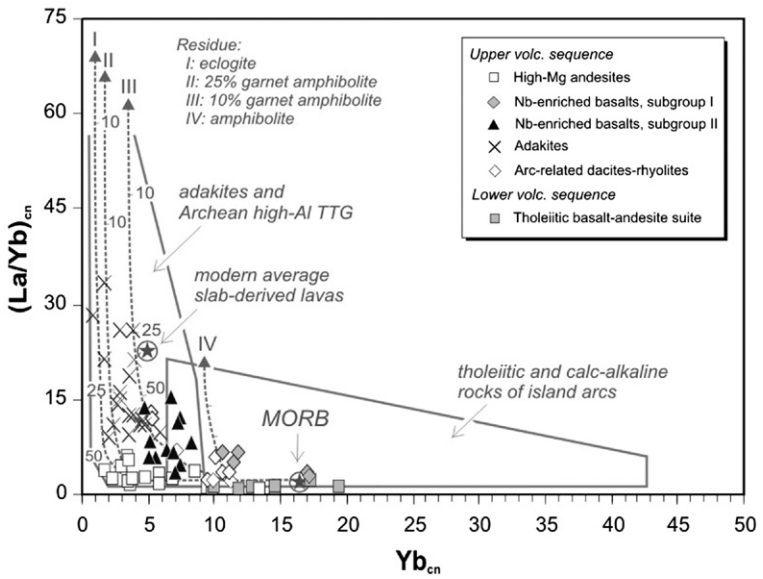


Fig. 14. $(La/Yb)_N$ *vs* Yb_N diagram (Martin, 1986) of volcanic rocks of the Tireo Fm. Samples of high-Mg andesites and basalts, Nb-enriched basalts and andesites and adakites are compatible with garnet-bearing residues after dehydration melting of eclogites or amphibolites. See text for discussion.

7.4. Petrogenesis of adakites and high-Mg andesites

Adakites are characterized by ≥56 wt.% SiO_2, ≥15 wt.% Al_2O_3, usually <3 wt.% MgO (rarely >6 wt.%), high Cr, Ni and Na contents ($3.5 \leq Na_2O \leq 7.5$ wt.%), low Y and HREE (e.g., Yb<1.8 ppm, Y<18 ppm), high Sr (rarely <400 ppm) and low abundance of HFSE (Martin et al., 2005). The dacites and rhyolites of the upper volcanic sequence of the Tireo Fm are comparable to above values (Table 1), except for Al_2O_3 and Na_2O in some samples, probably mobilized by alteration. Also, the coeval high-Al, Hbl-bearing tonalite dykes share the fractionated REE and low Yb contents of these adakitic dacites and rhyolites. According to Drummond et al. (1996) and Rapp et al. (2003), adakites are considered to represent slab melting with a garnet-amphibole to eclogitic residue. In Fig. 14, adakite compositions are consistent with 25–50% degree of melting of basalts leaving residual assemblages of eclogite and >10% garnet amphibolite. Non-adakitic dacites/rhyolites are low-pressure melts (<8 kbar) of amphibolites, formed by lower crustal anatexis in an intra-oceanic arc. Removal of sub-aluminous hornblende and garnet, either as restite or during early high-pressure crystallization, produce the high-Al, low-Yb compositions typical of adakites. Trends to high MgO, Cr, Co, and Ni can be accounted for the interaction between ascending siliceous slab-melts and the peridotitic subarc mantle wedge (Kelemen et al., 1990), and this is also responsible for variable SiO_2 contents (Martin et al., 2005). In this scenario, high-Mg andesites likely form by progressive hybridization of adakite liquids with metasomatized peridotite, which accounts for their "normal" character of high MgO, Cr, Ni, Th and Ce contents, compared with low Yb (0.4–1.1) and pronounced negative Nb and Ti anomalies (Kelemen, 1995; Yogodzinski et al., 1995, 2001). These reactions processes are expressed on the variation diagrams (Fig. 8) and Yb_{cn} *vs* $(La/Yb)_{cn}$ plot (Fig. 14), by the compositional continuity from tholeiitic basalts and andesites, through Nb-enriched basalts and andesites mixed with adakite-type liquids (Nb-rich dacites) to high-Mg andesites and end-member adakites.

7.5. Petrogenesis of Nb-enriched basalts and andesites

High-Nb (>20 ppm) and Nb-enriched basalts (6–20 ppm) are defined by Nb contents considerably greater than typical intra-oceanic arc basalts (Martin et al., 2005). Nb-enriched basalts of the Tireo Fm originated from a relatively enriched mantle source, because they have LREE-enriched patterns (Fig. 10), relatively high Nb contents (5–16 ppm) and low Zr/Nb ratios (7.4–22). This enrichment has been ascribed to plume-related sources (Leat et al., 2004), involvement of partial melting of subducted slab material (Pearce and Peate, 1995), or melting of peridotite previously metasomatized by slab-melts (Kepezhinskas et al., 1996; Sajona et al., 1996). The Nb-enriched basalts of the upper volcanic sequence differ from plume-related tholeiites (OIB and E-MORB-types of Sun and McDonough, 1989), in having a nearly flat or less fractionated HREE pattern, lower Nb/La and higher Gd/Yb ratios (Gd/Yb<2.5 *vs* 3.5). In the Gd/Yb *vs* Nb/La diagram (Fig. 15), Nb-enriched basalts samples plot below the Caribbean–Colombia oceanic plateau field (data from Hauff et al., 2000; Lapierre et al., 2000; Kerr et al., 2002), and other plume-related units in the Cordillera Central, as the Duarte Complex and the Siete Cabezas Fm. These characteristics suggest a different source for Nb-enriched basalts than those of the Caribbean plume-related lavas.

Several studies have addressed the spatial and temporal association in arcs of "normal" arc volcanics, high-Mg andesites, Nb-enriched basalts and adakites (Defant et al., 1991; Yogodzinski et al., 1995; Sajona et al., 1996, 1997; Yogodzinski et al., 2001; Tatsumi and Hanyu, 2003). The Nb-enriched basalt-adakite association results from the following events: (1) adakite liquids form by slab melting during subduction of young, hot oceanic lithosphere; (2) these liquids may erupt, or react with subarc mantle wedge peridotites, resulting adak-type high-Mg andesite or, if reaction proceeds further, SiO_2-depleted transitional adakites (Martin et al., 2005); (3) the mantle is metasomatically altered by the adakite liquids to an amphibole+ilmenite,

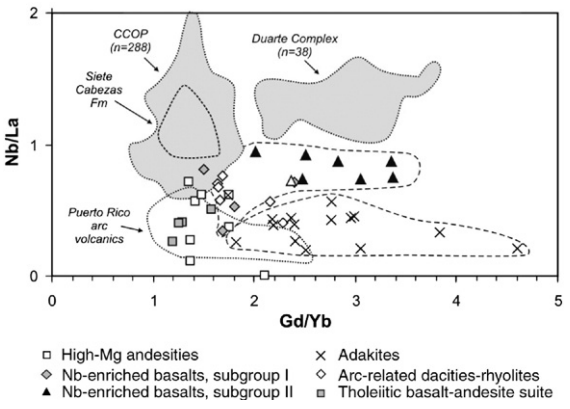


Fig. 15. Gd/Yb *vs* Nb/La diagram discriminating: (a) volcanic rocks of the Tireo Fm and OIB-like basalts (enriched mantle sources) from the Caribbean–Colombian oceanic plateau (data from Hauff et al., 2000; Lapierre et al., 2000; Kerr et al., 2002), Duarte Complex and Siete Cabezas Fm (Escuder Viruete et al., unpublished data), and Puerto Rico arc volcanics (Jolly et al., 1998, 2001).

or amphibole + Fe-rich orthopyroxene assemblage that scavenges HFSE from the liquid; and (4) induced convection in the subarc mantle drags the metasomatized peridotite to depths where it melts, generating Nb-enriched liquids (Kepezhinskas et al., 1996).

7.6. Geological evolution of the Tireo Fm

As the previous geological and geochemical data indicate, the Tireo Fm record an extended episode of complex volcanic and associated sedimentary activity in the suprasubduction zone setting of the Caribbean island arc. The earliest geological event is an Albian–Cenomanian period of submarine epiclastic sedimentation that produced at least 200 m of sandstone-turbidites and polymictic pebble and boulder debris-flow conglomerates, with interbedded volcanically-derived mudstones and tuffaceous black-shales (Río Blanco Mb). Gabbroic, Hbl-bearing tonalitic, basaltic and fossiliferous limestone clasts suggest that exhumed both arc-root plutons and effusive and sedimentary supracrustal rocks were present in their source areas. The overlying rocks of the lower volcanic sequence consist of a >2500-thick accumulation of very monotonous and extensive andesitic tuffs, with interbedded flows of tholeiitic basalts. Fossil and geochronological data show that arc magmatism began to accumulate before 90 Ma, from the Albian to Turonian. These pyroclastics were generated in a submerged island arc setting, developed over a substrate composed of Upper Jurassic MORB-type oceanic crust and a Lower Cretaceous Duarte Complex oceanic plateau. Due to compositional and temporal similarities, the lower volcanic sequence of the Tireo Fm record the same stage of island arc development that the upper basaltic unit of the Los Ranchos Fm. However, the stratigraphic base of the sequence is not exposed, and a considerable earlier (pre-Albian) geological history may be missing.

After a sedimentation interval of limestones (Constanza Mb) and cherts, the onset of upper sequence volcanism characterized by contemporaneous adakites, high-Mg andesites and Nb-enriched basalts, took place at Turonian–Coniacian boundary (~ 89 Ma) and continued in the Santonian to Lower Campanian. Explosive volcanism with sub-aerial and episodic aerial eruptions, sub-volcanic emplacements of rhyolitic domes and subseafloor hydrothermal systems, characterize this stratigraphic interval. The associated sediments contain mudstone, limestone and chert, and suggest a low volcanic relief. Along-strike changes in the stratigraphic disposition and lithologic composition of the Tireo Fm, in particular the absence of the lower volcanic sequence or the presence of limestone or chert members, are interpreted to result from non-deposition, stratigraphic pinch-out or structural termination and excision. It is suggested that active arc rifting may account for the overall architecture of the basin in which the upper unit was deposited, in particular the direct juxtaposition, near the northeastern basin margin (Santiago Rodríguez–Monción–Jarabacoa areas), of some of the oldest rocks in the formation or its Duarte Complex substrate, beneath the rhyolites of the upper volcanic sequence (El Yujo Mb; Fig. 3). In this respect, Escuder Viruete et al. (2006a) describe a sinistral strike-slip shearing and faulting deformation affecting the Tireo Fm and older rocks in the Cordillera Central, which was active during the 88–74 Ma interval. This deformation formed regional transpressional and transtensional structures, and was coeval with the intrusion of syn- to late-kinematic Loma de Cabrera tonalitic batholith (90–74 Ma), petrogenetically similar to the felsic volcanics of the upper volcanic sequence. Therefore, this deformation could be a cause of the lateral stratigraphic pinch-out or structural termination of the lower sequence and to define the basin geometry during the sedimentation of the upper sequence. After some episodic volcanism, the shallow-marine limestones of the Bois de Lawrence Fm were deposited in the Late Campanian–Maastrichtian on top of the arc.

7.7. Tectonic setting of the Tireo Fm

Any model proposed for the magmatic and tectonic evolution of the Tireo Fm has to explain the following observations: (1) normal tholeiitic magmatic products until 90 Ma, derived from melting of the mantle wedge above the slab; (2) 88–74 Ma active strike-slip shearing deformation that deform the volcanic arc; and (3) post-90 Ma, and thus syn- to late-kinematic eruption of adakites derived from melting of the subducting slab, and related high-Mg andesites and Nb-enriched basalts, which collectively record a major change in the composition of the erupted lavas. In order to explain these observations, a model of SW-directed, proto-Caribbean oblique ridge subduction at ~ 90 Ma is proposed as principal cause of tectonic and magmatic variations in the Hispaniola segment of the Caribbean island arc during the Late Cretaceous (Fig. 16). When a ridge is subducted, the forearc tend to become heated, intruded by magma and deformed, and the arc tends to be extinguished or invaded by magmas of anomalous composition, often triggered by a slab window formation (Hole et al., 1991; Cole and Basu, 1995; Thorkelson and Breitsprecher, 2005). Specifically, the main magmatic effects of ridge subduction and subsequent slab window is that “normal” arc volcanism is interrupted in the vicinity of the slab

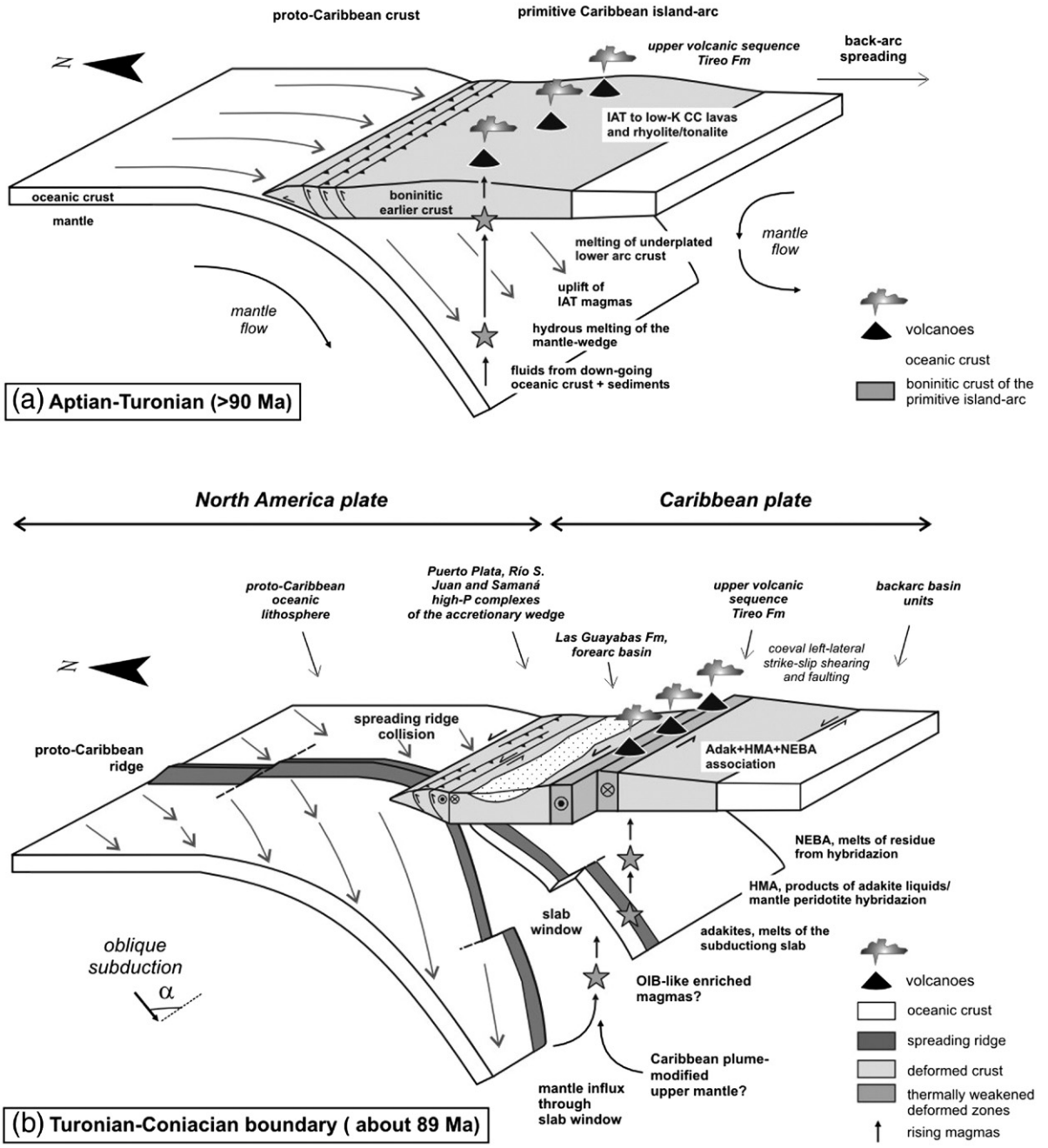


Fig. 16. Schematic tectonomagmatic model for the evolution of the volcanic rocks of the Tireo Fm. (a) SW-directed subduction of the proto-Caribbean crust beneath the primitive Caribbean island arc in Hispaniola. The lower volcanic sequence rocks constitute an island arc tholeiitic suite, derived from melting by fluxing of a mantle wedge (fertile MORB mantle) with subduction-related hydrous fluids. (b) Collision between the proto-Caribbean ridge and Caribbean island arc trench at ~ 89 Ma, and the probably formation of the slab window caused normal arc magmatism to stop. The Proto-Caribbean spreading ridge possibly was oriented at high-angle (see recent tectonic reconstructions of Pindell et al., 2005). Consequences are: (1) Adakite magmatism started after the slab window had formed. These magmas may have formed by melting at the leading edge of the subducting proto-Caribbean ridge. Related high-Mg andesites are the product of hybridization of adakite liquids with mantle peridotite, and Nb-enriched basalts/andesites melts of the residue from hybridization; (2) The upwelling of enriched deep mantle through the slab window (additional heat source) may therefore have facilitated proto-Caribbean ridge melting by heating the slab edge; (3) Collision and slab window formation may both have caused deformation in the arc by a combination of transpressional/transtensional and thermal processes; and (4) The evolution of a slab window predicts the appearance of OIB-type magmas and the possible influence of the Caribbean plume flowing northeastern into the mantle wedge.

window, and replaced by a broader but often less voluminous volcanic field of wide-range compositions, including those indicative of slab anatexis. The slab is progressively younger and hotter toward the subducting ridge, and the mantle within the slab window will tend to be hotter and less hydrated (Thorkelson and Breitsprecher, 2005). In these conditions, adakitic melts consequently form proximal to the proto-Caribbean plate edges at depths of 25–90 km (i.e. from garnet amphibolite to eclogite facies). Adventive heating from the ridge and upward mantle flow can also trigger re-melting of lithospheric mantle wedge previously metasomatized by slab-melts to form high-Mg andesites and Nb-enriched basalts.

An issue open to question is if ridge subduction was accompanied by slab window formation. In this situation, mantle upwelling through the slab window can produce more alkaline magmas in arc to back-arc locations, including those with OIB-type compositions (Hole et al., 1991; D'Orazio et al., 2001). Also, possible influence of the Caribbean mantle plume in source enrichment by flowing northeastern into the mantle wedge should not be discarded. To prove these hypothesis, future research in the Central Cordillera of Hispaniola will consist to test if the Late Cretaceous geological units with enriched geochemical characteristics, as the Pelona–Pico Duarte Basalts, Peña Blanca and Siete Cabezas Fm, were temporary and spatially related.

8. Conclusions

The Tireo Fm is composed of two volcanic sequences: the lower dominated by andesitic submarine vitric–lithic tuffs and volcanic breccias, with interbedded basaltic flows; and the upper by a genetic association of adakites, high-Mg andesites, and Nb-enriched basalts. The lower volcanic sequence constitute an island arc tholeiitic suite, derived from melting by fluxing of a mantle wedge with subduction-related hydrous fluids. In contrast, adakites likely represent melts of the subducting slab, magnesian andesites the product of hybridization of adakite liquids with mantle wedge peridotite, and Nb-enriched basalts/andesites melts of the residue from hybridization. We propose a model of SW-directed, oblique ridge subduction at ~ 90 Ma (Turonian–Coniacian boundary) as principal cause of the shift in the composition of the erupted lavas in the Caribbean island arc.

Acknowledgements

The authors would like to thank John Lewis (George Washington University) and Gren Draper (Florida International University) for the initial field-work and discussions and advice on the petrology and geochemistry of arc-related volcanic rocks in the Dominican Republic. This work forms part of the geothematic cartographic project of the Dominican Republic funded by the SYSMIN program of the European Union and received financial aid from MCYT projects BTE-2002-00326 and CGL2005-02162/BTE. Javier Montes (SYSMIN) is also thanked by field and administrative assistance. Also, we wish to thank Dirección General de Minería for the support in Dominican Republic. Reviews from G.M. Yogodzinski and an anonymous reviewer are much appreciated, as well as the editorial assistance of Stephen Foley.

Appendix A. Supplementary data

Supplementary data associated with this article can be found, in the online version, at doi:10.1016/j.lithos.2007.01.008.

References

Bienvenu, P., Bougault, H., Joron, J.L., Treuil, M., Demitriev, L., 1990. REE/non REE element hygromagmaphile element fractionation. Chemical Geology 82, 1–14.

Bourdon, E., Eissen, J.P., Monzier, M., Robin, C., Martin, H., Cotten, J., Hall, M.L., 2002. Adakite-like lavas from Antisana (Ecuador); evidence from slab melt metasomatism beneath the Andean northern volcanic zone. Journal of Petrology 43, 199–217.

Bowin, C., 1975. The geology of Española. In: Naim, A., Stehli, F. (Eds.), The ocean basins and margins: the Gulf of Mexico and the Caribbean, vol. 3. Plenum Press, New York, pp. 501–552.

Calmus, T., Aguillon-Robles, A., Maury, R.C., Bellon, H., Benoit, M., Cotten, J., Bourgois, J., Michaud, F., 2003. Spatial and temporal evolution of basalts and magnesian andesites (bajaites) from Baja California, Mexico: the role of slab melts. Lithos 66, 77–105.

Cole, R.B., Basu, A.R., 1995. Nd–Sr isotope geochemistry and tectonics of ridge subduction and middle Cenozoic volcanism in western California. Geological Society of America Bulletin 107, 167–179.

Contreras, F., Ardévol, Ll., Granados, L., Calvo, J.P., Escuder Viruete, J., Escuer, J., Florido, P., Antón Pacheco, C., García Lobón, J.L., Mortensen, J.K., Ullrich, T., Friedman, R., 2004. Mapa Geológico de la República Dominicana E. 1:50.000, Jicomé (5973-IV). Dirección General de Minería, Santo Domingo. 158 pp.

Defant, M.J., Drummond, M.S., 1990. Derivation of some modern arc magmas by melting of young subducted lithosphere. Nature 347, 662–665.

Defant, M.J., Richerson, P.M., de Boer, J.Z., Stewart, R.H., Maury, R.C., Bellon, H., Defant, M.J., Clark, L.F., Stewart, R.H., Drummond, M.S., de Boer, J.Z., Maury, R.C., Bellon, H., Jackson, T.E., Restrepo, J.F., 1991. Andesite and dacite genesis via contrasting processes: the geology and geochemistry of El Valle volcano, Panama. Contributions to Mineralogy and Petrology 106, 309–324.

Donnelly, T.W., Beets, D., Carr, M.J., Jackson, T., Klaver, G., Lewis, J., Maury, R., Schellenkens, H., Smith, A.L., Wadge, G., Westercamp, D., 1990. History and tectonic setting of Caribbean magmatism. In: Dengo, G., Case, J. (Eds.), The Caribbean Region. The Geology of North America, vol. H. Geological Society of America, pp. 339–374.

D'Orazio, M., Agostini, S., Innocenti, F., Haller, M.J., Manetti, P., Mazzarini, F., 2001. Slab window-related magmatism from southernmost south America; the late Miocene mafic volcanics from the Estancia Glencross area (approximately 52 degrees S. Argentina–Chile). Lithos 57, 67–89.

Draper, G., Lewis, J.F., 1991. Metamorphic belts in Central Española. In: Mann, P., Draper, G., Lewis, J.F. (Eds.), Geologic and Tectonic Development of the North America–Caribbean Plate Boundary in Española. Geological Society of America Special Paper, vol. 262, pp. 29–46.

Drummond, M.S., Defant, M.J., 1990. A model for trondhjemite–tonalite–dacite genesis and crustal growth via slab melting: Archean to Modern comparisons. Journal of Geophysical Research 95, 21503–21521.

Drummond, M.S., Defant, M.J., Kepezhinskas, P.K., 1996. Petrogenesis of slab-derived trondhjemite–tonalite–dacite/adakite magmas. In: Brown, M., Candela, P.A., Pecket, D.L. (Eds.), Third Hutton Symposium on the Origin of Granites and Related Rocks, Special Paper, vol. 315. Geological Society of America, Boulder, CO, pp. 205–215.

Escuder Viruete, J., Contreras, F., Stein, G., Urien, P., Joubert, M., Bernardez, E., Hernáiz Huerta, P.P., Lewis, J., Lopera, E., Pérez-Estaún, A., 2004. La secuencia magmática Jurásico Superior-Cretácico Superior en la Cordillera Central, República Dominicana: sección cortical de un arco-isla intraoceánico. Geotemas 6 (1), 41–44.

Escuder Viruete, J., Contreras, F., Stein, G., Urien, P., Joubert, M., Ullrich, T.D., Mortensen, J., Pérez-Estaún, A., 2006a. Transpression and strike-slip partitioning in the Caribbean island arc: fabric development, kinematics and Ar–Ar ages of syntectonic emplacement of the Loma de Cabrera batholith, Dominican Republic. Journal of Structural Geology 28, 1496–1519.

Escuder Viruete, J., Díaz de Neira, A., Hernáiz Huerta, P.P., Monthel, J., García Senz, J., Joubert, M., Lopera, E., Ullrich, T., Friedman, R., Mortensen, J., Pérez-Estaún, A., 2006b. Magmatic relationships and ages of Caribbean island-arc tholeiites, boninites and related felsic rocks, Dominican Republic. Lithos 90, 161–186.

Escuder Viruete J., Pérez-Estaún A., Contreras F., Joubert M., Weis D., Ullrich T.D., Spadea P. in press. Plume mantle source heterogeneity through time: insights from the Duarte Complex, Central Hispaniola. Journal of Geophysical Research.

Gómez Sáinz, A., 2000. Mapa Geológico de la República Dominicana E. 1:50.000, Constanza (6072). Dirección General de Minería, Santo Domingo. 230 pp.

Gradstein, F.M., Ogg, J.G., Smith, A.G., 2004. A Geologic Time Scale 2004. Cambridge University Press. 610 pp.

Hauff, F., Hoernle, K.A., Van den Bogaard, P., Alvarado, G.E., Garbe-Schínberg, C.D., 2000. Age and geochemistry of basaltic complexes in western Costa Rica: contributions to the geotectonic of Central America. Geochemistry, Geophysics, Geosystems 1 1999gc000020.

Hole, M.J., Rogers, G., Saunders, A.D., Storey, M., 1991. Relation between alkalic volcanism and slab window formation. Geology 19, 657–660.

Jolly, W.T., Lidiak, E.G., 2006. Role of crustal melting in petrogenesis of the Cretaceous Water Island Fm (Virgin Islands northeast Antilles island arc). Geologica Acta 4, 7–33.

Jolly, W.T., Lidiak, E.G., Dickin, A.K., Wu, T.W., 1998. Geochemical diversity of Mesozoic island arc tectonic blocks in eastern Puerto Rico. In: Lidiak, E.G., Larue, D.K. (Eds.), Tectonics and geochemistry of the northeastern Caribbean. Geological Society of America Special Paper, vol. 322, pp. 67–98.

Jolly, W.T., Lidiak, E.G., Dickin, A.K., Wu, T.W., 2001. Secular geochemistry of Central Puerto Rican island arc lavas: constraints on mesozoic tectonism in the eastern Greater Antilles. Journal of Petrology 42, 2197–2214.

Kelemen, P.B., 1995. Genesis of high Mg# andesites and the continental crust. Contributions to Mineralogy and Petrology 120, 1–19.

Kelemen, P.B., Johnson, K.T.M., Kinzier, R.J., 1990. High-field-strength element depletions in arc basalts due to mantle magma interaction. Nature 345, 521–552.

Kepezhinskas, P.K., Defant, M.J., Drummond, M.S., 1996. Progressive enrichment of island arc mantle by melt–peridotite interaction inferred from Kamchatka xenoliths. Geochimica Cosmochimica Acta 60, 1217–1229.

Kerr, A.C., Tarney, J., Kempton, P.D., Spadea, P., Nivia, A., Marriner, G.F., Duncan, R.A., 2002. Pervasive mantle plume head heterogeneity: evidence from the late Cretaceous Caribbean–Colombian oceanic plateau. Journal of Geophysical Research 107 (B7) (10.1029).

Lapierre, H., Dupuis, V., de Lepinay, B.M., Bosch, D., Monie, P., Tardy, M., Maury, R.C., Hernandez, J., Polve, M., Yeghicheyan, D., Cotten, J., 1999. Late Jurassic oceanic crust and upper cretaceous Caribbean plateau picritic basalts exposed in the Duarte igneous complex, Hispaniola. Journal of Geology 107, 193–207.

Lapierre, H., Bosch, D., Dupuis, V., Polvé, M., Maury, R., Hernandez, J., Monié, P., Yeghicheyan, D., Jaillard, E., Tardy, M., de Lepinay, B., Mamberti, M., Desmet, A., Keller, F., Senebier, F., 2000. Multiple plume events in the genesis of the peri-Caribbean Cretaceous oceanic plateau province. Journal of Geophysical Research 105, 8403–8421.

Leat, P.T., Pearce, J.A, Barker, P.F., Millar, I.L., Barry, T.L., Larter, R.D., 2004. Magma genesis and mantle flow at a subducting slab edge: the South Sandwich arc–basin system. Earth and Planetary Science Letters 227, 17–35.

Lebrón, M.C., Perfit, M.R., 1994. Petrochemistry and tectonic significance of Cretaceous island-arc-rocks, Cordillera Oriental, Dominican Republic. Tectonophysics 229, 69–100.

Lewis, J.F., Amarante, A., Bloise, G., Jimenez, J.G., Dominguez, J., 1991. Lithology and stratigraphy of Upper cretaceous rocks volcanic and volcaniclastic rocs of the Tireo Group, Dominican Republic and correlations with the Massif du Nord with Haiti. In: Mann, P., Draper, G., Lewis, J.F. (Eds.), Geologic and tectonic development of the North America–Caribbean plate boundary in Hispaniola. Geological Society of America Special Paper, vol. 262, pp. 143–163.

Lewis, J.F., Escuder Viruete, J., Hernaiz Huerta, P.P., Gutiérrez, G., Draper, G., 2002. Subdivisión Geoquímica del Arco Isla Circum-Caribeño, Cordillera Central Dominicana: Implicaciones para la formación, acreción y crecimiento cortical en un ambiente intraoceánico. Acta Geológica Hispánica 37, 81–122.

Mann, P., 1999. Caribbean Sedimentary Basins: Classification and Tectonic Setting from Jurassic to Present. In: Mann, P. (Ed.), Caribbean Basins. Sedimentary Basins of the Word, vol. 4, pp. 3–31.

Martin, H., Smithies, R.H., Rapp, R., Moyen, J.F., Champion, D., 2005. An overview of adakite, tonalite–trondhjemite–granodiorite (TTG), and sanukitoid: relationships and some implications for crustalevolution. Lithos 79, 1–24.

Maury, R.C., Sajona, F.G., Pubellier, M., Bellon, H., Defant, M.J., 1996. Fusion de la croûte océanique dans les zones de subduction/collision récentes; l'exemple de Mindanao (Philippines). Bulletin de la Société Geologique de France 167, 579–595.

McCarron, J.J., Smellie, J.L., 1998. Tectonic implications of forearc magmatism and generation of high-magnesian andesites: Alexander Island, Antarctica. Journal of the Geological Society (London) 155, 269–280.

Montgomery, H., Pessagno, E.A., 1999. Cretaceous microfaunas of the Blue mountains, Jamaica, and of the Northern and Central

Basement Complexes of Hispaniola. Caribbean. In: Mann, P. (Ed.), Caribbean Basins. Sedimentary Basins of the Word, vol. 4 (10), pp. 237–246.

Pearce, J.A., Parkinson, I.J., 1993. Trace element models for mantle melting: application to volcanic arc petrogenesis. In: Pritchard, H.M., Alabaster, T., Harris, N.B.W., Nearly, C.R. (Eds.), Magmatic processes and plate tectonics. Geological Society of London Special Publication, vol. 76, pp. 373–403.

Pearce, J.A., Peate, D.W., 1995. Tectonic implications of the composition of volcanic arc magmas. Earth and Planetary Science Annual Rewiew 23, 251–285.

Pindell, J.L., Kennan, L., Maresch, W.V., Stanek, K.P., Draper, G., Higgs, R., 2005. Plate-kinematics and crustal dynamics of circum-Caribbean arc-continent interactions: tectonic controls on basin development in Proto-Caribbean margins. In: Lallemant, A., Sisson, V.B. (Eds.), Caribbean–South American Plate Interactions. Geological Society America Special Paper, vol. 394, pp. 7–52.

Polat, A., Kerrich, R., 2001. Magnesian andesites, Nb-enriched basalt-andesites, and adakites from late-Archean 2.7 Ga Wawa greenstone belts, Superior, Superior Province, Canada: implications for late Archean subduction zone petrogenetic processes. Contribution to Mineralogy and Petrology 141, 36–52.

Rapp, R.P., Shimizu, N., Norman, M.D., 2003. Growth of early continental crust by partial melting of eclogite. Nature 425, 605–609.

Sajona, F.G., Maury, R., Bellon, H., Cotten, J., Defant, M.J., 1996. High field strength element enrichment of Pliocene–Pleistocene island arc basalts, Zamboanga Peninsula, western Mindanao (Philippines). Journal of Petrology 37, 693–726.

Sajona, F.G., Bellon, H., Maury, R., Pubellier, M., Quebral, R., Cotten, J., Bayon, F., Pagado, E., Pamatian, P., 1997. Tertiary and Quaternary magmatism in Mindanao and Leyte (Philippines); geochronology, geochemistry and tectonic setting. Journal of Asian Earth Sciences 15, 121–153.

Smith, I.E.M., Worthington, T.J., Steward, R.B., Price, R.C., Gamble, J.A., 2003. Felsic volcanism in the Kermadec arc, SW Pacific: crustal recycling in an oceanic setting. In: Laster, R.B., y Leat, P.T. (Eds.), Intraoceanic Subduction Systems: Tectonic and Magmatic Processes. Geological Society London Special Publication, vol. 219, pp. 99–118.

Stein, G., Ardévol, Ll., Bourdillon, Ch., Bonnemaison, M., Escuder Viruete, J., Le Goff, E., Escuer, J., Lopera, E., Antón Pacheco, C., García Lobón, J.L., Mortensen, J.K., Ullrich, T., Friedman, R., 2004. Mapa Geológico de la República Dominicana a E. 1:50.000, Restauración (5873-I). Dirección General de Minería, Santo Domingo. 168 pp.

Stern, R.J., 2002. Subduction zones. Reviews of Geophysics 40, 867–1012. doi:10.1029/2001RG000108.

Sun, S.S., McDonough, W.F., 1989. Chemical and isotopic systematics of oceanic basalts: implications for mantle compositions and processes. In: Saunders, A.D., Norry, M.J. (Eds.), Magmatism in the Ocean Basins. Geological Soc Special Publication, vol. 42, pp. 313–345.

Tamura, Y., Tatsumi, Y., 2002. Remelting of an andesitic crust as a possible origin for rhyolitic magma in oceanic arcs: an example from the Izu–Bonin arc. Journal of Petrology 43, 1029–1047.

Tatsumi, Y., 1989. Migration of fluid phases and genesis of basalt magmas in subduction zones. Journal of Geophysical Research 94, 4697–4707.

Tatsumi, Y., Eggins, S., 1995. Subduction Zone Magmatism. Blackwell Science, Cambridge, MA, p. 211.

Tatsumi, Y., Hanyu, T., 2003. Geochemical modeling of dehydration and partial melting of subducting lithosphere: toward a comprehensive understanding of high-Mg andesite formation in the Setouchi volcanic belt, SW Japan. Geochemistry, Geophysics, Geosystems 4, 1081.

Thorkelson, D.J., Breitsprecher, K., 2005. Partial melting of slab window margins: genesis of adakitic and non-adakitic magmas. Lithos 79, 25–41.

Yogodzinski, G.M., Kay, R.W., Volynets, O.N., Koloskov, A.V., Kay, S.M., 1995. Magnesian andesite in the western Aleutian Komandorsky region: Implications for slab melting and processes in the mantle wedge. Geological Society of America Bulletin 107, 505–519.

Yogodzinski, G.M., Lees, J.M., Churikova, T.G., Dorendorf, F., Woerner, G., Volynets, O.N., 2001. Geochemical evidence for the melting of subducting oceanic lithosphere at plate edges. Nature 409, 500–504.